SPECIFIC ABSORPTION RATE ASSESSMENT IN A HUMAN HEAD MODEL EXPOSED TO RADIATION FROM CELLULAR PHONE

by

Binay Özsoy Demirbilek

B.S. in Electronic and Communication Engineering
Istanbul Technical University, 1988

Submitted to the Institute of Biomedical Engineering
in partial fulfillment of the requirements
for the degree of
Master of Science
in
Biomedical Engineering

Boğaziçi University
June, 2001

ACKNOWLEDGEMENTS

The work presented here was performed in the Institute of Biomedical Engineering of Boğaziçi University under the supervision of Prof. Dr. Ş.Selim Şeker and supported by the Boğaziçi University Research Foundation Project No: 00A201.

I would like to express my sincere gratitude and deep thanks to my thesis advisor Prof. Dr. Ş.Selim Şeker, who proposed this subject to me, for his precious contributions and support throughout this study.

I would like to thank also Prof. Dr. Avni Morgül, Funda Akleman and Levent Sevgi for their contributions.

I am also thankful to the staff of the Institute of Biomedical Engineering, especially to Prof. Dr. Yorgo Istefanopulos for their support.

Finally, I would like to express my best wishes to my family, especially my daughters to whom I have devoted all my life.

SPECIFIC ABSORPTION RATE ASSESSMENT IN A HUMAN HEAD MODEL EXPOSED TO RADIATION FROM CELLULAR PHONE

ABSTRACT

The increasing use of electromagnetic (EM) devices has caused growing concern about possible health hazards produced by EM radiation. So it is imperative to be able to quantify both the absorption of electromagnetic energy in the human body and the resulting thermal effect.

In this study, the specific absorption rate of radiofrequency radiation (900 MHz) from cellular phones on the human head was investigated. A comprehensive review of the available data on EM radiation safety standards and electrical properties of human tissues was added.

The electrical properties of the tissues are generally frequency dependent. Thermal properties are, in contrast, fixed and can simply be adapted from research literature on hyperthermia.

As it is not possible to perform the experiments on human in vivo, we simulated the human head and the antenna radiated in 900 MHz. Two geometrical models for the head can be considered, namely the spherical model and the realistic head model. In this study the spherical model with a single layer and three layers was simulated by using the Agilent High Frequency Structure Simulator, which employs the finite element method (FEM), and the EM power absorption rate of tissue was calculated by a C++ program. The results were compared with the results of the studies in the literature performed by using Finite Difference Time Domain Method and Moment Method and Green's Function and great agreement was obtained.

Keywords: Specific Absorption Rate (SAR), Electromagnetic radiation, Finite Element Method (FEM)

CEP TELEFONUNDAN KAYNAKLANAN IŞIMAYA MARUZ KALAN BİR İNSAN KAFASINDA ENERJİ SOĞURULMA ORANININ DEĞERLENDİRİLMESİ

ÖZET

Elektromanyetik cihazların kullanımlarının hızla artması, bilimadamlarını elektromanyetik (EM) radyasyonun insan sağlığı üzerindeki etkilerini araştırmaya yöneltmiştir. Bu amaçla yapılan araştırmalarda elektromanyetik enerjinin insan dokuları tarafından soğurulması ve termal etkileri somut bir şekilde belirlenmeye çalışılmaktadır.

Bu çalışmada, 900 MHz'te çalışan cep telefonundan yapılan ışımaya maruz kalan bir insan kafasının enerji soğurma oranı incelenmiştir. EM radyasyon ile ilgili güvenlik standartları ve insan dokusunun elektriksel özellikleri de çalışmaya eklenmiştir.

İnsanlar üzerinde deneyler yapılamadığı için kobaylar üzerinde deney yapmak veya bilgisayar ortamında insanı modellemek ve olayları simüle etmek mümkündür. Bu çalışmada, yüksek frekanslarda anten modellemek için geliştirilmiş Agilent Yüksek Frekans Yapı Simülatör'ü kullanılarak dipol anten ile insan kafası tek ve üç katlı olarak modellenmiş ve yazılan bir C++ programı yardımı ile program sonucu elde edilen elektrik alan değerlerinden enerji soğurulma katsayısı (Specific Absorption Rate, SAR) elde edilmiştir. Agilent Yüksek Frekans Yapı Simülatör'ü, 3-boyutlu ortamda Maxwell Denklemlerini Sonlu Elemanlar Metodu (Finite Elements Method, FEM) ile çözmektedir. Bu yöntemle elde edilen sonuçlar, literatürde Sonlu Farklar, Moment Metodu ve Green Fonksiyonu ile elde edilmiş sonuçlarla karşılaştırılmıştır. Karşılaştırma sonuçları uygulanan bu yöntemin güvenilir olduğunu göstermektedir.

Anahtar Sözcükler: Enerji Soğurulma Oranı (SAR), Elektromanyetik enerji, Sonlu Elemanlar Metodu (FEM)

TABLE OF CONTENTS

Page

ACKNOWLEDGEMENTS iii

ABSTRACT iv

ÖZET v

TABLE OF CONTENTS vi

LIST OF FIGURES viii

LIST OF TABLES x

LIST OF ABBREVIATIONS AND SYMBOLS xi

1. INTRODUCTION 1

1.1. Background of the Problem 1

1.2. Literature Review 3

1.3. Medical Safety Standards 7

1.4. The Structure of the Thesis 12

2. RF RADIATION AND THE ELECTRICAL PROPERTIES OF BIOLOGICAL TISSUES 13

2.1. Biological Effects of RF Radiation on the Human Head 13

2.2. Electrical Properties of Biological Tissue 18

3. THE FINITE-ELEMENT-METHOD AND AGILENT HIGH-FREQUENCY STRUCTURE SIMULATOR 25

3.1. The Finite Element Method 25

3.2. Agilent HFSS 30

4. MODELING A HUMAN HEAD AND AND CELLULAR PHONE ANTENNA WITH AGILENT HFSS SOFTWARE 33

4. 1. Multilayered Spherical Model of a Human Head 33

4.2. Modeling Dipole Antenna 35

4.3. Simulation 37

4.4. SAR Computation 38

4.5. Simulation Results 39

4.5.1. The Dipole Antenna 39

4.5.2. The Single-Layered Spherical Human Head 41

4.5.3. The Three-Layered Spherical Human Head 47

4.5.4. The Three-Layered Ellipsiod Rat Model 50
4.6. The Comparison of the Results with the Literature 55
4.6.1. The Comparison of the Human Head Models 55
4.6.2. The Comparison of the Rat Models 56
5. CONCLUSION 58
APPENDIX The Flowchart of C++ Program 59
REFERENCES 60
REFERENCES NOT CITED 65

LIST OF FIGURES

		Page
FIGURE 2.1	Radiation Pattern With Antenna	15
FIGURE 2.2	Frequency dependence of the dielectric constant of muscle tissue	19
FIGURE 2.3	Dielectric properties of muscle in the impedance plane, with reactance X plotted against resistance R and the impedance $Z = R + jX$.	20
FIGURE 2.4	Equivalent circuit for the β-dispersion of a cell suspension and corresponding plot in the complex dielectric constant plane	22
FIGURE 3.1	Circle discretized into 5 "elements" and 5 "nodes"'	28
FIGURE 3.2	Local approximation of arc length on each "element"	29
FIGURE 3.3	A tetrahedron	31
FIGURE 4.1	Plane wave incident upon spherical model with six concentric shells	33
FIGURE 4.2	a) The antenna model used in study	35
	b) The location of antenna	36
FIGURE 4.3	a) Geometry of the equivalent dipole antenna and human head	36
	b) The model drawn in HFSS software package	37
FIGURE 4.4	Finite Element Mesh	38
FIGURE 4.5	The far field of antenna	40
FIGURE 4.6	The horizontal cut of far field	40
FIGURE 4.7	The normalized magnitude of the electric field (V/m) along the axes.	41
FIGURE 4.8	The far field patterns of the antenna with single-layered human head model	42
FIGURE 4.9	The 2D cross-section patterns of the far field	43
FIGURE 4.10	The normalized magnitude of the electric field (V/m) along the axes.	44
FIGURE 4.11	The distribution of local SAR values in the planes	44

FIGURE 4.12	The far field pattern of the antenna with three-layered human head model	47
FIGURE 4.13	The 2D cross-section pattern of the far field	47
FIGURE 4.14	The distribution of local SAR values in the planes	48
FIGURE 4.15	The model of the rat and the antenna	50
FIGURE 4.16	The far field patterns the antenna with three-layered rat model	51
FIGURE 4.17	The 2D cross-section patterns of the far field	51
FIGURE 4.18	The normalized magnitude of the electric field (V/m) along the axes.	53
FIGURE 4.19	The distribution of local SAR values in the planes	53
FIGURE 4.20	a) Radiation pattern obtained by Nikita b) Radiation patterns in our study	56

LIST OF TABLES

		Page
TABLE 1.1	Basic restrictions for time varying electric and magnetic fields for frequencies up to 10 GHz	9
TABLE 1.2	Limits of Specific Absorption Rate (Continuous Exposure) 10 kHz-300 GHz	10
TABLE 1.3	Reference levels for workers and general public exposure to time-varying electric and magnetic fields (rms values)	11
TABLE 2.1	Bands of radio frequency and subradio-frequency fields and radiation	13
TABLE 2.2	Dielectric constant of various body tissues at 37°C	23
TABLE 2.3	Conductivity in $m\Omega^{-1}$/cm of various tissues at 37°C	23
TABLE 2.4	Properties of electromagnetic waves in biological media (fat, bone)	23
TABLE 2.5	Properties of electromagnetic waves in biological media (muscle, skin)	24
TABLE 4.1	Tissues and radius used for six concentric shell model	34
TABLE 4.2	The tissues and the properties used in simulations	35
TABLE 4.3	Antenna Parameters	39
TABLE 4.4	Some of SAR values in the single-layered spherical human head	46
TABLE 4.5	Some of SAR values in the three-layered spherical human head	50
TABLE 4.6	The tissues and the properties used in simulations	51
TABLE 4.7	Some of local SAR values in the three-layered ellipsoid rat-head modeling	54
TABLE 4.8	Comparison of the peak SAR values of human head models	55
TABLE 4.9	Comparison of the peak SAR values of rat models	57

LIST OF ABBREVIATIONS AND SYMBOLS

E	Electric field intensity
H	Magnetic field intensity
μ	Permeability
ε	Permittivity
σ	Conductivity
SAR	Specific Absorption Rate
ρ	Density of tissue
f	Frequency
ω	Radial frequency
Umax	Maximum Radiation Intensity
FEM	Finite Element Method
MoM	Method of Moment

1. INTRODUCTION

The increasing use of electromagnetic (EM) devices has caused growing concern about possible health hazards produced by EM radiation. So, it is imperative to be able to quantify both the absorption of EM energy in the human body and the resulting thermal responses.

The most investigated effect of EM energy on biological tissues is the transformation of energy entering the tissues into increased kinetic energy of the absorbing molecules, thereby producing a general heating in the medium. The power absorbed by the tissues will produce a temperature rise that is dependent on the cooling mechanism of the tissue. The patterns of the fields producing the heating are complex functions of the frequency, source configuration, tissue geometry and dielectric properties of the tissues. When the thermoregulatory capability of the system is exceeded, tissue damage results.

In this thesis, a complete electromagnetic analysis was performed considering the head of a subject exposed to cellular phones. The finite-element method was used to solve the Maxwell's equations and specific absorption rate (SAR) in models of a human head.

1.1 Background of the Problem

The electric field is produced by a changing magnetic field and the magnetic field is produced by a changing electric field. The first of these concepts resulted from experimental research by Michael Faraday and the second from the theoretical efforts of James Clerk Maxwell. In 1864, James Clerk Maxwell proposed mathematically that energy can be transferred by electric and magnetic fields traveling together at a finite speed. It was not until 1886, however, that Heinrich Hertz experimentally proved Maxwell's theory of electromagnetism. To accomplish this, Hertz constructed the first oscillator-transmitter. This consisted of two metal spheres that were each connected to the end of a rod that had a spark gap in the center. The receiving antenna consisted of a loop with a tiny gap cut into it. With this equipment, Hertz conducted experiments that demonstrated the similarity between radio waves and light waves, and the polarization, refraction, and reflection of EM waves. Although Hertz's experiments were performed with relatively short wavelength

radiation (50 and 450 megahertz [MHz]), later work in radio was performed at longer wavelengths.

The Maxwell's time-dependent curl equations in differential forms are;

$$\nabla \times E = -\mu \frac{\partial H}{\partial t} \tag{1.1}$$

$$\nabla \times H = \sigma E + \varepsilon \frac{\partial E}{\partial t} \tag{1.2}$$

Where;

E: Electric field (V/m)
H: Magnetic field (A/m)
μ: permeability
ε: permittivity
σ: conductivity

When a biological system is exposed to microwave radiation, an internal field is induced in the system. The calculation of this internal field is named dosimetry [1]. The electromagnetic energy absorbed per unit mass of tissue is called specific absorption rate (SAR) [1]:

$$SAR = \frac{\sigma}{2\rho} E_i^2 \tag{1.3}$$

Where;

ρ: density of tissue (kg/m^3)
E_i: internal electrical field (V/m)

To solve the internal electric field problems, there are two approaches:

1. Analytical methods, in which the EM field equations are solved directly, and

2. Numerical techniques, which are characterized by the numerical solution of large systems of simultaneous equations.

The calculation of the internal field is difficult to achieve because of many dependent factors; therefore, mathematical techniques that consist of numerically solving Maxwell's equations for reasonably accurate representations of the actual objects are generally used in the computer simulation. In numerical techniques, Maxwell's equations can be solved as a set of linear equations by matrix inversion or by iterative techniques. Generally, two numerical methods are employed:

1. The moment method

2. Finite-element or finite difference approaches

The moment method has been utilized to calculate localized SAR's in block model representations of humans. The accuracy of these moment method solutions is very difficult to establish. To improve the accuracy of the solution, finite-element method with tetrahedral elements can be used. To reduce the long computation time, which is required in this technique, the finite-difference approach is useful. Since the number of operations is proportional to the square of the number of elements in the matrix, solving the large system of equations is very slow. Therefore, finite-difference methods allow a more realistic model to be constructed [2,3].

The spherical model approximates the primate cranial structure irradiated by plane wave in the cellular frequencies range. The simplest problem of this type is that of a plane wave falling upon a homogeneous sphere. This problem was first solved by Mie and was concisely presented by Stratton. A solution for the scattering coefficients from a sphere with one concentric shell was given by Aden and Kerker and the inhomogeneous spherically symmetric object was calculated by Wyatt.

1.2 Literature Review

The development of models to predict the absorption of electromagnetic energy and the physiologic thermoregulatory response for the human body has proceeded for several years. Some of these studies are summarized here as follows:

In 1986, Arthur W. Guy et al. studied on quantification of the SAR-patterns in human models exposed to UHF mobile-antenna fields using thermography, nonperturbing temperature probes and E-field sensitive diodes [4]. The exposure conditions included

man, woman, and child models in different positions. In this study, full-scale phantom models, which were filled with synthetic gel having the same dielectric properties as human muscles, were used. The result of this study was "the mobile-antenna system could be operated safely with all of the ANSI RFPG exposure guides [5] in terms of both power density and maximum SAR".

In 1978, Quirino Balzano et al. measured energy deposition in simulated human tissue exposed for one minute in the vicinity of a 800 MHz portable radio transmitter [6]. Two different phantoms were used: the flat phantom and the head phantom consisting of a real human skull stuffed with simulated brain tissue. The deposited energy was evaluated by temperature measurements. It was found that no thermal damage to tissue was caused by normal use of the portable radio.

In 1994, Macfarlane measured the free-space near E-field close to a 2 W GSM digital mobile telephone inside a large semi-anechoic shielded chamber [7]. In this study, an indication of the peak near E-field, which is applied to a hearing aid, was also provided.

In 1993, Toftgard et al., investigated the effects of the presence of a person on the performance of antennas for cellular telephones [8]. In this study, it was shown that input impedance, far-field radiation pattern, radiation efficiency and the magnitude of the near-field were affected by the presence of the human body. FDTD technique was applied. The hand and the head were modeled as pure muscle.

In 1994, Chen et al. investigated the current and SAR distributions in an inhomogeneous model of a human head exposed to the EM waves irradiated from a cellular phone by using the FDTD method [9]. In this study, the human head was simulated by a model of 57263 block cells with inhomogeneous dielectric constant and conductivity. It was found that the maximum SAR induced in the head was below the IEEE upper safety limit.

In 1996, Lu et al. used FDTD and FD methods to calculate electromagnetic thermal simulations of a 3D human head model under RF radiation [10]. For human head modeling, MR images were used. The calculated peak temperature rise was 0.15 °C and in the study, the long term biological influence of this rise on the human head was indicated to be considerable.

In 2000, L.W. Li et al. studied interactions between five commercial handset antennas and human-head tissue in personal communications by using the FDTD method [11]. Heterogeneous and realistic head models were used to calculate the SAR values. For the heterogeneous model, the anatomical features of the human head and hand were modeled within the FDTD framework by mapping the spatial location of the different tissues into a permittivity and conductivity assignment in the computational grid. The result of this study was that the SAR values for the monopoles and the side-mounted PIFA exceeds the safety limits stipulated by the ANSI/IEEE Safety Guide lines if the users continuously communicate using headsets for over an hour.

In 2000, Bernardi et al. did electromagnetic and thermal analysis on human heads exposed to various kinds of cellular phones focusing the attention on important organs like the eye lens and brain [1]. In this study, magnetic resonance images were used for modeling the human head and hand. For all the considered phone models, a maximum SAR value of 1.6 W/kg gave rise to a temperature increase in the brain of about 0.09 °C, which is about 50 times lower than the threshold for thermal damage.

In 2000, Wang and Fujiwara investigated the role of head tissue complexity in the peak SAR assessment for cellular phones by using the FDTD method in conjuction with a realistic human head model based on MRImages [12]. 17 different types of tissue of the head were the subject of the study and it was indicated that different antenna types caused different SAR values but in the meantime it was also reported that the 5-tissue head model was sufficient to obtain accurate peak values.

In 2000, Drossos et al. studied SAR values of head tissue for the frequency range of 300-3000 MHz [13]. Multilayered structure model and the 4-Cole-Cole formula for calculation of dielectric properties were used in the study; the final tests were conducted on the basis of different MRI-based nonhomogeneous human head phantoms. The spatial-peak SAR values of the homogeneous model were larger than those of nonhomogeneous models.

In 2000, Schiavoni et al. studied SAR values generated by cellular phones inside an anatomical model of a head [14]. To solve the electromagnetic problem, the FDTD method was used. The results were compared with the SAR values of 4 different (homogeneous and nonhomogeneous) types of phantom. The SAR values for each model were different.

In 2000, Nikita et al. studied interaction between a Layered Spherical Head Model and a finite-length dipole antenna by the method based on the combination of the Green's function method with the MAS (method of auxiliary sources) [15].

In 2000, Iskander et al. investigated the effect of the body on the microwave absorption in a human head exposed to radiation from a cellular phone [16]. Head and body were modeled by mapping the spatial location of the different tissues and the FDTD method was used to solve the electromagnetic problems. Tests were conducted with both monopole and PIFA antennas. The antenna orientation was also examined. It was shown that neglecting the effect of the body resulted in underestimating SAR Values by 53%.

In 2000, Mason et al, studied the effects of frequency, permittivity and voxel size on the SAR values [17]. The researchers emphasized that the role of thermoregulatory components (e.g. conduction, convection, and blood flow) in determining the increase in temperature during EMF exposure should be taken into account.

In 2000, Stevens and Martens investigated the effects of the average volume (its geometry and size) on SAR values and found that the applied criterion caused a variation of 20%-30% in the SAR values [18].

In 2000, Okana et al. introduced a biotic tissue-equivalent solid phantom as the human head model realizing the same relative dielectric constant and conductivity as brain tissue and skull layer [19]. The FDTD method was used for calculation and the thermographic method for comparison.

In 2000, Lozzi et al. used the perfectly matched layer (PML) boundary to truncate a 3-mm resolution head model used for cellular phone simulations [20]. This approach reduced the FDTD space in the ear-to-ear, back-to-front and bottom-to-top directions by embedding the exposed sides of the head in PM Layers. This approach was found appropriate for SAR accuracy at the lower frequency range. This study also showed that by using the truncated half-model, it was possible to obtain accurate radiation patterns at frequencies of 835 and 1900 MHz.

In 2000, Mangoud et al. combined the frequency-domain method of moments (MoM) and FDTD for the simulation of human interaction with cellular phones [21]. The

results of the tests were in excellent agreement with published results and expectations. This method was useful for analyzing complex problems.

On the other hand, medical researchers have been studying thermal effects and changes on the ear. In one of these studies, W.S. Noyes and al. reported that moderate changes in cochlear temperature (3-4 degrees) of rabbits did not produce irreversible thermal damage to the cochlear outer hair cells [22]. W. Keck and al. studied conduction of thermal stimuli in the human temporal bone [23] and reported that the temperature difference across the horizontal semicircular canal was of shorter duration than the absolute temperature change.

As it can be seen, the studies on electromagnetic radiation of cellular phones on the human head were performed either by using the FDTD, FD, Moment Method or phantoms. In our study, the FEM was used and compared with the literature.

1.3 Medical Safety Standards

Caused by the tremendous expansion of the use of electricity in all aspects of life, the problems raised by the influence of Electromagnetic Fields on human beings become more and more important. The non-negligible possibility of adverse health effects on humans leads to a need for regulations for the prevention of the effects. These regulations cover two aspects: the biological/medical aspect with regard to the user and the technical aspect with regard to the sources of EM fields and their measurement.

The standardisation organisations define in principle three kinds of regulations:

-standards, which are precise documents and should be strictly applied,

-recommendations, the application of which allows some flexibility,

-guides, guidelines, which are rather informative documents and the application of which is also less compulsory.

In 1998 new guidelines were issued by ICNIRP, the International Committee on Non-Ionizing Radiation Protection, linked to the World Health Organization [24]. These guidelines are based on an extensive survey of research results, mainly of a biomedical

nature. The guidelines apply to exposure levels. They define levels to which the following categories of individuals can be exposed: the general public and occupational workers.

ICNIRP distinguishes two categories of the values:

-Basic Restrictions. Although they include a safety factor, ICNIRP considers the basic restrictions as upper limits for exposure. The Basic Restrictions are expressed in the quantities B magnetic flux density (T), J current density (A/m^2), SAR specific absorption rate (W/kg), and S power density (W/m^2) as they occur in the human body.

In the frequency range of about 1 MHz to a few GHz the specific absorption rate (SAR) is the significant dosimetric quantity for establishing exposure limits. The threshold for effects considered detrimental to health is observed at 4 W/kg, averaged over the whole body (Table 1.1). Healthy people at rest, in light clothing and in environmental conditions of 20 – 22 °C and relative humidity of up to 50% with adequate ventilation seem able to dissipate RF power at SARs of up to 4 W/kg, without increasing the systemic temperature by more than 1 °C. The level of peak power deposition into the body for exposures longer than 30 μs is 333 W/kg and 67 W/kg for workers and the general public respectively.

-Reference Levels. These are developed because some of the Basic Restrictions are difficult to measure in the human body. The Reference Levels are derived from the Basic Restrictions under worst-case conditions, such as maximum coupling of the exposed fields into the human body. The Reference Levels are expressed in E electric field strength (V/m), H magnetic field strength (A/m), B (Tesla), S (W/m^2), I_L limb current (A), I_C contact current (A), for pulsed fields SA (specific energy absorption J/kg).

Table 1.1
Basic restrictions for time varying electric and magnetic fields for frequencies up to 10 GHz [24]

Exposure Characteristics	**Frequency Range**	**Current density for head and trunk (mA/m^2)**	**Whole-body average SAR (W/kg)**	**Localized SAR (head and trunk) (W/kg)**	**Localized SAR (limbs) (W/kg)**
Occupational Exposure	up to 1 Hz	40	-	-	-
	1-4 Hz	40/f	-	-	-
	4 Hz-1 kHz	10	-	-	-
	1-100 kHz	f/100	-	-	-
	100 kHz-10 MHz	f/100	0.4	10	20
	10 MHz-10 GHz	-	0.4	10	20
General Public Exposure	up to 1 Hz	8	-	-	-
	1-4 Hz	8/f	-	-	-
	4 Hz-1 kHz	2	-	-	-
	1-100 kHz	f/500	-	-	-
	100 kHz-10 MHz	f/500	0.08	2	4
	10 MHz-10 GHz	-	0.08	2	4

Based on the ICNIRP guidelines The Council of Health Ministers of the European Union issued the Council Recommendation on the limitation of exposure of the general public to electromagnetic fields (0 to 300 GHz) on 12 July 1999 [25]. This recommendation advises the member states to adopt it into national legislation. Within five years the European Commission will report the adoption.

In Turkey, between 1995 and 1998 European Prestandards for Low Frequency (0 Hz to 10 kHz) ENV 50166-1 and High Frequency (10 kHz to 300 GHz) ENV 50166-2 [26,27] were approved as prospective standards for provisional applications. While reference levels of induced current densities, contact currents, electric and magnetic fields were defined for each frequency level for the frequencies between 0 and 10 kHz, Specific Absorption Rate (SAR) was added for frequencies between 10 kHz and 300 GHz. The limits are summarized as below:

Table 1.2
Limits of Specific Absorption Rate (Continuous Exposure), 10 kHz-300 GHz [27]

	SAR averaged over any 6 min. time interval and over the whole body	SAR averaged over any 6 min. time interval and any 10 g of tissue other than hands, wrists, feet, ankles	SAR averaged over any 6 min. time interval and 10 g of tissue in the hands wrists, feet ankles	Peak SA averaged over any 10 g of tissue
Workers	0,4 W/kg	10 W/kg	20 W/kg	10 mJ/kg
General Public	0,08 W/kg	2 W/kg	4 W/kg	2 mJ/kg

The comparison of values of ENV 50166-2 and ICNIRP for high frequencies is given in Table 1.3. From this table, it is clearly understood that there is no significant difference between these two standards for high frequencies.

In 1998, The European Specification ES 59005 [28] was announced but not yet approved by the Institute of Turkish Standards. In this specification, the SAR values were the same as ENV 50166-2 [27] and ICNIRP [24] and detailed data on a great number of existing systems were provided.

Table 1.3

Reference levels for workers and general public exposure to time-varying electric and magnetic fields (rms values) [13,16]

Frequency	ENV 50166-2 Prestandards				ICNIRP Guidelines			
	Electric field Strength (RMS) (V/m)		Magnetic Field Strength (RMS) (A/m)		Electric field Strength (RMS) (V/m)		Magnetic Field Strength (RMS) (A/m)	
	Workers	General Public	Workers	General Public	Workers	General Public	Workers	General Public
10-38 kHz	1000	400	42	16,8	610	87	24,4	5
38-150 kHz	1000	400	1,6/f	0,7/f	610	87	1,6/f	5
150-610 kHz	1000	400	1,6/f	0,7/f	610	87	1,6/f	0,73/f
610 kHz- 1MHz	614/f	275/f	1,6/f	0,7/f	610	87	1,6/f	0,73/f
1-10 MHz	614/f	275/f	1,6/f	0,7/f	610/f	87/ $f^{1/2}$	1,6/f	0,73/f
10-400 MHz	61,4	27,5	0,16	0,07	61	28	0,16	0,073
400-2000 MHz	3,07 $f^{1/2}$	1,37 $f^{1/2}$	0,00814 $f^{1/2}$	0,00364 $f^{1/2}$	3 $f^{1/2}$	1,375 $f^{1/2}$	0,008 $f^{1/2}$	0,0037 $f^{1/2}$
2-150 GHz	137	61,4	0,364	0,163	137	61	0,36	0,16
150-300 GHz	0,354 $f^{1/2}$	0,158 $f^{1/2}$	0,00094 $f^{1/2}$	0,000421 $f^{1/2}$	137	61	0,36	0,16

1.4 The Structure of the Thesis

In this thesis, in chapter 1, the problem with the literature survey and the medical safety standards are declared; the electrical parameters (conductivity and dielectric constant) used in modeling human head are reviewed in chapter 2; some brief information is given about Finite-Element-Method (FEM) in chapter 3; and spherical model of human head with the results of simulation by using Agilent HFSS software, which employs the FEM in simulation, is investigated in chapter 4.

In chapter 4, the verification of the model is also examined by comparing the results with the literature.

The thesis is concluded in chapter 5.

2. RF RADIATION AND THE ELECTRICAL PROPERTIES OF BIOLOGICAL TISSUE

In this chapter, we will summarize the EM radiation and two electrical properties that define the electrical characteristics of tissues, namely, the dielectric constant relative to free space (ε) and conductivity (σ).

2.1 Biological Effects of EM Radiation on the Human Head

Radiofrequency electromagnetic radiation (EMR), a form of energy between 10 KHz-300 GHz in the electromagnetic spectrum, is used in wireless communication and emitted from antennae of mobile telephones and from cellular masts.

Table 2.1
Bands of radio frequency and subradio-frequency fields and radiation

Frequency Range	Wavelength Range	Name
>300 GHz	<1 mm	Infrared
30 GHz--300 GHz	10 mm--1 mm	Extremely high frequency (EHF)
>3 GHz--30 GHz	10 cm--1 cm	Superhigh frequency (SHF)
300 MHz--3 GHz	1 m --10 cm	Ultra high frequency (UHF)
30 MHz--300 MHz	10 m--1 m	Very high frequency (VHF)
3 MHz--30 MHz	100 m--10 m	High frequency (HF)
300 kHz--3 MHz	1 km--100 m	Medium frequency (MF)
30 kHz--300 kHz	10 km--1 km	Low frequency (LF)
3 kHz--30 kHz	100 km--10 km	Very low frequency (VLF)
300 Hz--3 kHz	1000 km--100 km	Voice frequency
>0--300 Hz	≥1000 km	Extremely low frequency (ELF)
0 Hz	--	Static

Frequencies>300 MHz up to 300 GHz are referred to as "microwaves".
Frequencies >3000 kHz up to 300 GHz are referred to as "radiofrequencies". Lower frequencies are referred to as "subradiofrequencies".
A traditional definition of extremely low frequencies was frequencies between 30 Hz and 300 Hz.

Wireless communication systems operate at several frequencies in the electromagnetic spectrum. In the United States, cell phones operate in two main frequency ranges; the older systems near 850 MHz, and the newer personal communication services, or PCS, near 1900 MHz. European Mobile phones use the Global System for Mobile Communication (GSM), a different technology than most U.S. phones and operate at slightly different frequencies, near 900 MHz and 1800 MHz.

Energy in this frequency range is called non-ionizing because the photon energy is insufficient to knock electrons from atoms in living tissue, unlike a source of serious biological damage from radiation such as X-rays.

The most apparent biological effects of EM energy at cell phone frequencies are due to heating. EM radiation can penetrate organic tissues and be absorbed and converted into heat. The close proximity of a mobile telephone antenna to the user's head leads to the deposition of a relatively large amount of electromagnetic energy in the head. The relatively fixed position of the antenna to the head causes a repeated irradiation of a more or less fixed amount of body tissue. Exposure to EMR from mobile telephones is of a short-term, repeated nature at a relatively high intensity. The biological and health consequences of these exposure conditions need further understanding.

Formal research on the biological effects of EMR began more than 30 years ago. However, knowledge of the possible health effects of EMR is still inadequate and inconclusive. The main barrier in understanding the biological effects of EMR is caused by the complex interaction of different exposure parameters causing an effect. An independent variable of such complexity is unprecedented in any other field of biological research.

The intensity (or power intensity) of EMR in the environment is measured in units such as mW/cm^2. However, the intensity provides little information on the biological consequence unless the amount of energy absorbed by the irradiated object is known. This is generally given as the specific absorption rate (SAR), which is the rate of energy absorbed by a unit mass (e.g., one kg of tissue) of the object, and usually expressed as W/kg.

The rate of absorption and the distribution of EMR energy in an organism depend on many factors. These include: the dielectric composition (i.e., ability to conduct electricity) of the irradiated tissue, e.g., bones, with a lower water content, absorb less of the energy than muscles; the size of the object relative to the wavelength of the EMR (thus,

the frequency); shape, geometry, and orientation of the object; and configuration of the radiation. The distribution of energy in the head of a user of a mobile telephone is more discrete because of the relatively stationary position of the phone. Depending on the size of the head and the frequency of the radiation, regions of relatively high absorption can occur at or near the center of the brain. These effects are especially uncontrollable in the near-field during the use of mobile communication devices like cordless and cellular phones and very unpredictable due to the variable shape, size, and thickness of skulls. The worst case scenario occurs when a cellular phone's antenna is held as close as possible to the temple or eyes. Thus, in summary, the pattern of energy absorption inside an irradiated body is non-uniform, and biological responses are dependent on distribution of energy and the body part that is affected. Different areas of the brain have different sensitivities to EMR. This further indicates that the pattern of energy absorption could be an important determining factor of the nature of the response. The figures below show the pattern that an EM wave radiated from a cellular phone follows [29].

Top View **Front View**

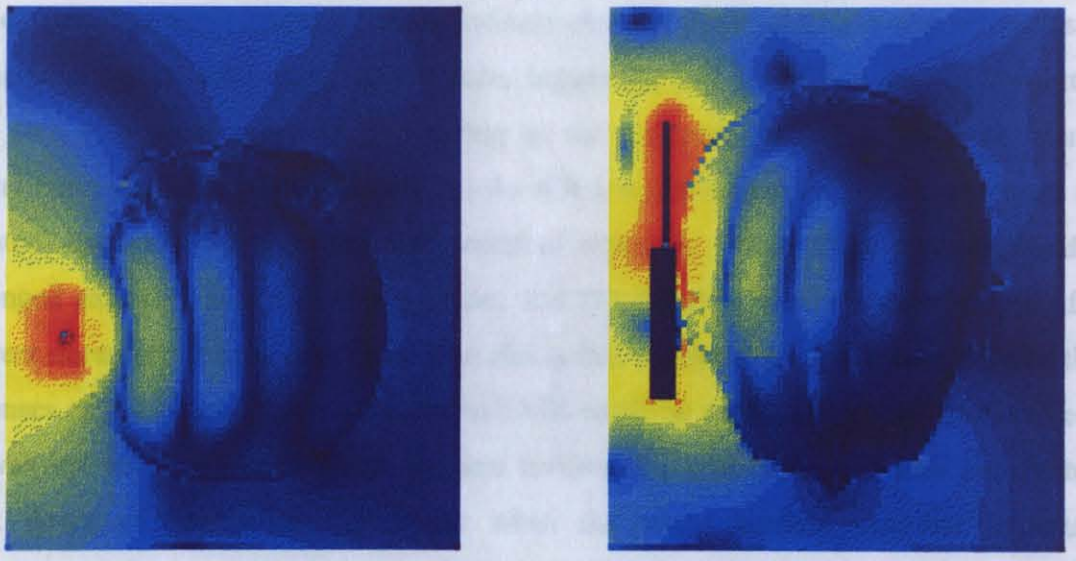

Figure 2.1 Radiation Pattern With Antenna [29]

Two obviously important parameters that will be focused on in this study are the frequency and intensity of EMR. The question of frequency is vital because it dictates whether existing research data on the biological effects of EMR can apply to the case of

mobile telephones. Most previous research studied frequencies different from those used in wireless communication.

It must be pointed out that data showing different frequencies producing different effects, or an effect that was observed at one frequency and not at another, are sparse. However, it is not certain whether these differences were actually due to differences in the distribution of energy absorption in the body exposed at the various frequencies. In addition, some studies showed frequency-window effects, i.e., effect is only observed at a certain range of frequencies and not at higher or lower ranges. These results may suggest that the frequency of an EMR can be a factor in determining the biological outcome of exposure.

An important question regarding the biological effects of EMR is whether the effects are cumulative, i.e., after repeated exposure, will the nervous system adapt to the perturbation and, with continued exposure, when will homeostasis break down leading to irreparable damage? The question of whether an effect will cumulate over time with repeated exposure is particularly important in considering the possible health effects of mobile telephone usage, since it involves repeated exposure of short duration over a long period (years) of time. Existing results indicate changes in the response characteristics of the nervous system with repeated exposure, suggesting that the effects are not 'forgotten' after each episode of exposure. Depending on the responses studied in the experiments, several outcomes have been reported. (1) An effect was observed only after prolonged (or repeated) exposure, but not after one period of exposure; (2) an effect disappeared after prolonged exposure suggesting habituation; and (3) different effects were observed after different durations of exposure. Related to this is that various lines of evidence suggest that responses of the central nervous system to EMR could be a stress response. Stress effects are well known to cumulate over time and involve first adaptation and then an eventual break down of homeostatic processes when the stress persists. Another important conclusion of the researches is that modulated or pulsed EMR seems to be more effective in producing an effect compared with continuous-wave radiation of the same frequency. In addition, in order to understand the biological consequence of EMR exposure, it must be known whether the effect is cumulative, whether compensatory responses result, and when homeostasis will break down.

When EMR is absorbed, it is converted into heat. A readily understandable mechanism of the effect of EMR is tissue heating (thermal effect). Biological systems alter their functions as a result of change in temperature. However, there is also a question of whether 'nonthermal' effects can occur from EM exposure. There can be two meanings to the term 'nonthermal' effect. It could mean that an effect occurs under the condition of no apparent change in temperature in the exposed tissue, suggesting that physiological or exogenous mechanisms maintain the exposed object at a constant temperature. The second meaning is that somehow EMR can cause biological effects without the involvement of heat energy (or it is temperature independent). This is sometimes referred to as 'athermal effect'. But it is very difficult to rule out thermal effects in biological responses to EMR, because it is difficult to reproduce the same pattern of internal heating of EMR by external heating since heat energy is inevitably released when EMR is absorbed. However, the pattern of energy distribution in the body is important in determining the effect of EMR. Another difficulty in eliminating the contribution of thermal effects is that it can be 'micro-thermal'. An example of this is the 'auditory effect' or 'electrophonic effect' of pulsed EMR. We can perceive a buzzing or clicking sound in the back of our heads; simply we can hear EMR delivered in pulses. An explanation for this 'hearing' effect is that it is caused by thermoelastic expansion of the head of the 'listener.' The absorbed energy produces a thermoelastic expansion of the brain tissue causing an acoustic pressure wave, which is detected in the cochlea by the hair cells of the organ of Corti. The threshold of hearing was determined to be approximately 10 microjoule/gm per pulse, which causes an increment of temperature in the head of one millionth of a degree centigrade.

When the nervous system or the brain is disturbed, e.g., by EMR, morphological, electrophysiological, and chemical changes can occur. A significant change in these functions will inevitably lead to a change in behavior. Indeed, neurological effects of EMR reported in the literature include changes in blood-brain-barrier, morphology, electrophysiology, neurotransmitter functions, cellular metabolism, calcium efflux, responses to drugs that affect the nervous system, and behavior. One common feature of these responses was that they seemed to be related to the activity of a group of neurotransmitters in the brain known as the endogenous opioids. These are compounds that are generated by the brain and behave like morphine. Increase in endogenous opioid activity in the brain can somehow cause alcohol-drinking behavior (Interactions between EMR with drugs could have important implications on the health effects of EMR. They

suggest that certain individuals in the population could be more susceptible to the effects of EMR).

Another interesting finding is that some of the effects of EMR are classically conditional. Conditioning processes, which connect behavioral responses with events (stimuli) in the environment, are constantly modifying the behavior observed by Pavlov. It's known that biological effects of EMR can be classically conditioned to cues in the exposure environment.

EMR can also affect memory functions. The effects are most likely reversible and transient.

Finally, it can be concluded that it is very difficult to deny that EMR at low intensity can affect the nervous system. However, data available suggest a complex reaction of the nervous system to EMR. Exposure to EMR does produce various effects on the central nervous system. The response is not likely to be linear with respect to the intensity of the radiation. Other parameters of EMR exposure, such as frequency, duration, waveform, frequency- and amplitude modulation, etc, are important determinants of biological responses and affect the shape of the dose (intensity)-response relationship. In order to understand the possible health effects of exposure to EMR from mobile telephones, one needs first to understand the effects of these different parameters and how they interact with each other.

2.2 Electrical Properties of Biological Tissue

Two electrical properties that define the electrical characteristics of tissues, namely, the dielectric constant relative to free space (ε) and conductivity (σ) are the subject of this section.

Both properties change with temperature and, strongly, with frequency. As a matter of fact, as the frequency increases from a few hertz to gigahertz, the dielectric constant decreases from several million to only a few units; concurrently, the conductivity increases from a few milliohms per centimeter to nearly a thousand.

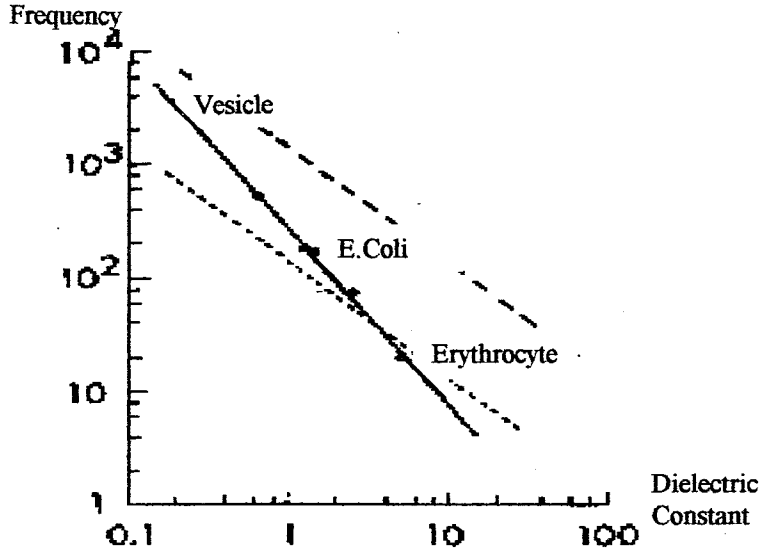

Figure 2.2 Frequency dependence of the dielectric constant of muscle tissue [30]

Figure 2.2 indicates the dielectric behavior of practically all tissues. Two remarkable features are apparent: exceedingly high dielectric constants at low frequencies and three clearly separated relaxation regions - α, β, and γ - of the dielectric constant at low, medium, and very high frequencies. Fine structural effects are responsible for deviations as indicated by the dashed lines.

α-dispersion : Variability with frequency of the apparent outer-cell membrane capacitances

β-dispersion : Maxwell-Wagner type relaxation resulting from the charging of cell membranes.

γ-dispersion : Dielectric relaxation of free water (f near 20 GHz)

The separation of the relaxation regions greatly aids in identifying the underlying mechanism. Inhomogeneous structure is responsible for the β-dispersion--the polarization resulting from the charging of interfaces (i.e. membranes through intra- and extracellular fluids: Maxwell-Wagner effect).

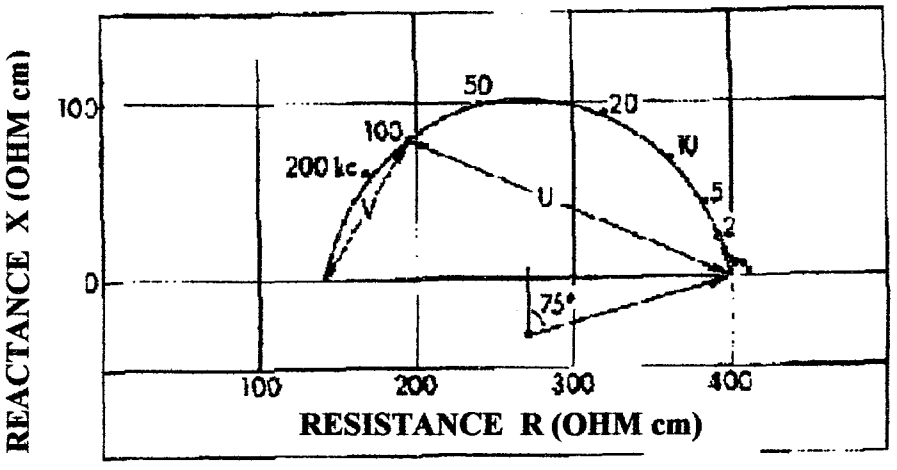

Figure 2.3 Dielectric properties of muscle in the impedance plane, with reactance X plotted against resistance R and the impedance Z = R + jX [30]. The large circle results from the β-dispersion and the small one from the α-dispersion. The plot does not include the γ-dispersion.

A typical example is presented in Figure 2.3 in the form of an impedance locus. The dielectric properties of muscle tissue are seen to closely conform to a suppressed circle, i.e. to a Cole-Cole distribution function of relaxation times. A small second circle at low frequencies represents the α-dispersion effect. Rotation of molecules having a permanent dipole moment, such as water and proteins, is responsible for the γ-dispersion (water) and a small addition to the tail of the β-dispersion resulting from a corresponding β_1 dispersion of proteins. The tissue proteins only slightly elevate the high-frequency tail of the tissue's β-dispersion because the addition of the β_1- effect caused by tissue proteins is small compared to the Maxwell-Wagner effect and occurs at somewhat higher frequencies. Another contribution to the β-dispersion is caused by smaller subcellular structures, such as mitochondria, cell nuclei, and other subcellular organelles. Since these structures are smaller in size than the surrounding cell, their relaxation frequency is higher but their total dielectric increment smaller. They therefore contribute another addition to the tail of the β-dispersion (β_1).

The γ-dispersion is due solely to water and its relaxational behavior is about 20 GHz.

The α-dispersion is presently the least clarified. Intracellular structures, such as the tubular apparatus in muscle cells that connect with the outer cell membranes could be responsible in tissues that contain such cell structures. Relaxation of counter ions around the charged cellular surface is another mechanism. Relaxational behavior of membranes per se, such as reported for the giant squid axon membrane, can account for the α-dispersion [31]. The relative contribution of the various mechanisms varies from one case to another and needs further elaboration.

Membranes are responsible for the dielectric properties of tissues and cell suspensions at RF's. Yeast, blood, bacteria, pleuropneumonia-like organisms (PPLO), vesicles, and cellular organelles have been extensively investigated by many investigators, including Fricke [32], Cole [33] and Schwan [34]. This work has led to a detailed understanding of the role of cell membranes in the polarization processes of biological media in the RF range. The principal mechanism for dielectric polarization at RF's and below is the accumulation of charges at membranes from extra- and intracellular fluids. For spherical particles, the following expressions were derived [34]:

$$\epsilon_s - \epsilon_\infty = \frac{9}{4\epsilon_r} \frac{\rho RC_m}{\left[1 + RG_m\left(\rho_i + \frac{1}{2}\rho_a\right)\right]^2} \rightarrow \frac{9}{4\epsilon_r}\rho RC_m \qquad (2.1)$$

$$\sigma_s = \sigma_a\left[1 - 1.5\rho\frac{1 + RM_m(\rho_i - \rho_a)}{1 + RM_m\left(\rho_i + \frac{1}{2}\rho_a\right)}\right] \rightarrow \sigma_a(1 - 1.5\rho) \qquad (2.2)$$

$$\sigma_\infty = \sigma_a\left[1 + 3\rho\frac{\sigma_i - \sigma_a}{\sigma_i + 2\sigma_a}\right] \qquad (2.3)$$

In these equations, C_m and G_m are capacitance and conductance per square centimeter of the cell membrane; R is the cell radius; ρ is the cellular volume fraction, and $\sigma_i = 1/\rho_i$ and $\sigma_a = 1/\rho_a$ are the conductivities of the cell interior and suspending medium. The equations apply for small-volume fractions, ρ, and assume that the radius of the cell is very large compared with the membrane thickness. A physical insight into the equations

above is gained by considering the equivalent circuit shown in Figure 2.4, which displays the same frequency response defined in these equations.

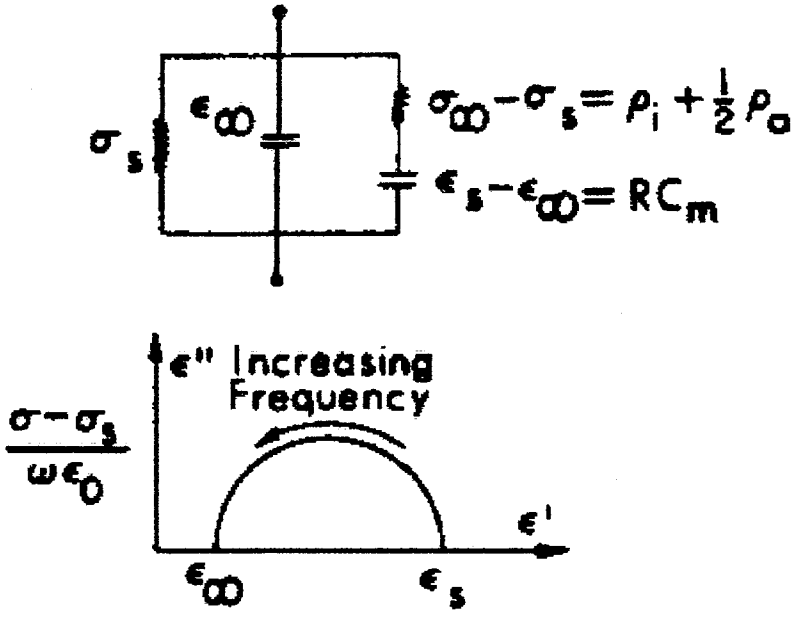

Figure 2.4 Equivalent circuit for the β-dispersion of a cell suspension and corresponding plot in the complex dielectric constant plane [35].

From the membrane capacitance, the values for the transmembrane potentials induced by microwave fields can be estimated. At frequencies well above the characteristic frequency (a few MHz), the membrane-capacitance impedance becomes very small by comparison with the cell-access impedance, and the membrane behaves electrically like a short circuit.

The analytic properties of the complex dielectric constant provide certain relationships between $\varepsilon_r'(\omega)$ and $\varepsilon_r''(\omega)$; they are not independent of each other. This relationship, known as the Kronig-Kramers relations can be written as follows:

$$\varepsilon'(\omega_c) = \varepsilon'(\infty) - \frac{2}{\pi} \int_0^{\infty} \frac{\omega\,\varepsilon''(\omega) - \omega_c\,\varepsilon''(\omega_c)}{\omega^2 - \omega_c^2}\, d\omega \qquad (2.4)$$

$$\varepsilon''(\omega_c) = \frac{\sigma(0)}{\varepsilon_0 \omega_c} - \frac{2\omega_c}{\pi} \int_0^{\infty} \frac{\varepsilon'(\omega) - \varepsilon'(\omega_c)}{\omega^2 - \omega_c^2}\, d\omega \qquad (2.5)$$

Dielectric constants of some body tissues are as follows: (Data were composed from Oswald, Schwan and Li).

Table 2.2
Dielectric constant of various body tissues at 37°C

Tissue	25 MHz	50 MHz	100 MHz	200 MHz	400 MHz	700 MHz	1000 MHz	3000 MHz	8500 MHz
Brain	>160	110-114	81-83	-	-	-	-	-	-
Fat	-	11-13	-	4.5-7.5	4-7	-	5.3-7.5	3.9-7.2	3.5-4.5
Muscle	103-115	85-97	71-76	56	52-54	52-53	49-52	45-48	40-42
Bone	-	6.8-7.7	-	-	-	-	4.3-7.3	4.2-5.8	4.4-5.4

Table 2.3
Conductivity in $m\Omega^{-}1/cm$ of various tissues at 37°C

Tissue	25 MHz	50 MHz	100 MHz	200 MHz	400 MHz	700 MHz	1000 MHz	3000 MHz	8500 MHz
Brain	4.55	4.76-5.26	5.13-5.56	-	-	-	-	-	-
Fat	-	0.4-0.59	-	0.29-0.95	0.36-11.1	-	0.83-1.49	1.11-2.27	2.7-4.17
Muscle	-	6.8-8.85	-	9.52-10.5	11.1-11.3	12.7-13.7	12.7-13.3	21.7-23.3	83.3
Bone	-	0.2-3.6	-	-	-	-	0.43-1	1.16-2.25	1.67-4.76

Table 2.4
Properties of electromagnetic waves in biological media (fat, bone)

Frequency (Mhz)	Dielectric Constant	Conductivity ($m\Omega^{-1}/m$)
27.12	20	10.9-43.2
40.68	14.60	12.6-52.8
100	7.45	19.1-75.9
200	5.95	25.8-94.2
300	5.70	31.6-107
433	5.60	37.9-118
750	5.60	49.8-138
915	5.60	55.6-147
1500	5.60	70.8-171
2450	5.50	96.4-213
3000	5.50	110-234
5000	5.50	162-309
5900	5.05	186-338
8000	4.70	255-431
10000	4.50	324-549

Table 2.5
Properties of electromagnetic waves in biological media (muscle, skin)

Frequency (Mhz)	Dielectric Constant	Conductivity ($m\Omega^{-1}/m$)
1	2000	0.4
10	160	0.625
27.12	113	0.612
40.68	97.3	0.693
100	71.7	0.889
200	56.5	1.28
300	54.0	1.37
433	53.0	1.43
750	52.0	1.54
915	51.0	1.60
1500	49.0	1.77
2450	47.0	2.21
3000	46.0	2.26
5000	44.0	3.92
5900	43.3	4.73
8000	4.00	7.65
10000	49.9	10.30

3. THE FINITE ELEMENT METHOD AND AGILENT HIGH-FREQUENCY STRUCTURE SIMULATOR

In this study, the Finite Element Method (FEM) is being utilized because the use of tetrahedral elements allows curved surfaces to be approximated much more accurately than is possible by the cubical blocks used in the Method of Moment and the Finite Difference Method. In this chapter, brief information about FEM and the software Agilent HFSS is given.

3.1 The Finite Element Method

The essence of the finite element method is to take a complex problem whose solution may be difficult if not impossible to obtain, and decompose it into pieces upon each of which a simple approximation of the solution may be constructed, and then put the local approximate solutions together to obtain a global approximate solution. The strategy is as follows:

- Subdivide [a,b] into n subintervals, called elements, that join at x_1, x_2,..., x_{n-1}. Add to this array x_0=a and x_n=b. We call the x_i the nodes of the interval. Number the elements from 1 to n where element (i) runs from x_{i-1} to x_i. The x_i need not be evenly spaced.
- Apply the Galerkin method (a residual method that uses weighting functions and computes the unknown coefficients by setting the integral over [a,b] of the weighted residual to zero) to each element separately to interpolate (subject to the differential equation) between the end nodal values, $u(x_{i-1})$ and $u(x_i)$, where these u's are approximations to the $y(x_i)$'s that are the true solution to the differential equation.
- Use a low-degree polynomial for u(x). Our development will use a first-degree polynomial, although quadratics or cubics are often used. (The development for these higher-degree polynomicals parallels is more complicated.)

- The result of applying Galerkin to the element (i) is a pair of equations in which the unknowns are the nodal values at the ends of element (i), the c's. When we have done this for each element, we have equations that involve all the nodal values, which we combine to give a set of equations that we can solve for the unknown nodal values. (The process of combining the separate element equations is called assembling the system.)
- These equations are adjusted for the boundary conditions and solved to get approximations to y(x) at the nodes; we get intermediate values for y(x) by linear interpolation [36].

Fundamental Notions

Global Coordinates: The real positions of every node in the chosen coordinates are called global coordinates. In the Cartesian coordinate system, the global coordinates of every node are given by (x_i, y_i, z_i).

Natural Coordinates: In the natural coordinate system, the position of any point of the element is defined by four coordinate values $_i$, i=1....4, called natural coordinates. In 3D space, the natural coordinates are defined with respect to the vertices of the tetrahedron element containing the point:

$$\zeta_i = V_i/V \quad , i = 1....4 \tag{3.1}$$

where V is the volume of the tetrahedron and V_i is the volume of the internal tetrahedra formed by the point and three of the vertices of the tetrahedron element excluding vertex number *i*. As such a definition implies, the natural coordinates are also called tetrahedron coordinates. Besides that, as the sum of internal tetrahedron volumes must be equal to the volume of the tetrahedron element, the natural coordinates are not completely independent of one another: That is;

$$\sum_{i=1}^{4} \zeta_i = 1 \tag{3.2}$$

Relations between Global and Natural Coordinates The global Cartesian coordinates and the natural coordinates are related by:

$$\begin{Bmatrix} x \\ y \\ z \\ 1 \end{Bmatrix} = \begin{bmatrix} x_1 & x_2 & x_3 & x_4 \\ y_1 & y_2 & y_3 & y_4 \\ z_1 & z_2 & z_3 & z_4 \\ 1 & 1 & 1 & 1 \end{bmatrix} \begin{Bmatrix} \zeta_1 \\ \zeta_2 \\ \zeta_3 \\ \zeta_4 \end{Bmatrix} \tag{3.3}$$

Interpolation Functions: Also called shape function, the interpolation functions can be expressed in a number of ways. The shape functions of a nth-order tetrahedron element can be expressed by the following systematic formula:

$$\alpha_{ijkl}(\zeta_1,\zeta_2,\zeta_3,\zeta_4) = P_i(\zeta_1)\, P_j(\zeta_2)\, P_k(\zeta_3)\, P_l(\zeta_4) \tag{3.4}$$

where

$$\begin{cases} P_m(z) = \prod_{i=1}^{m} \frac{Mz-i+1}{i}, & m \geq 1 \\ = 1, & m = 0 \end{cases} \tag{3.5}$$

The subscripts i, j, k, l are integers satisfying the constraint of

$$i + j + k + l = M \tag{3.6}$$

where *n* is the order of interpolation function. For 4-node tetrahedron element, the order of the interpolation function is M = 1. In that case, the interpolation functions are only defined at the 4 vertices of the tetrahedron:

$$\alpha_{1000}(\zeta_1,\zeta_2,\zeta_3,\zeta_4) = \zeta_1 \tag{3.7}$$

$$\alpha_{0100}(\zeta_1,\zeta_2,\zeta_3,\zeta_4) = \zeta_2 \tag{3.8}$$

$$\alpha_{0010}(\zeta_1,\zeta_2,\zeta_3,\zeta_4) = \zeta_3 \tag{3.9}$$

$$\alpha_{0001}(\zeta_1,\zeta_2,\zeta_3,\zeta_4) = \zeta_4 \tag{3.10}$$

For purpose of convenience, the interpolation functions in this case can be renumbered as m=1...4. In the case, m is called **multi-index**.

Geometric Constant The interpolations are given as functions of the local coordinates. The FEM formulations, as shown later, always start with global coordinates. Therefore, in part of the derivations, the interpolations functions may need to be expressed in terms of global coordinates. To do that, local coordinates must first be expressed in global coordinates in a simple manner:

$$\zeta_i\,(x,y,z) = \frac{(a_i + b_i x + c_i y + d_i z)}{3!V} \tag{3.11}$$

From the definition, it can be shown that

$$a_i = \frac{(-1)^{i-1}}{3!V}\begin{vmatrix} x_2 & y_2 & z_2 \\ x_3 & y_3 & z_3 \\ x_4 & y_4 & z_4 \end{vmatrix} \tag{3.12}$$

$$b_i = \frac{-(-1)^{i-1}}{3!V}\begin{vmatrix} 1 & y_2 & z_2 \\ 1 & y_3 & z_3 \\ 1 & y_4 & z_4 \end{vmatrix} \tag{3.13}$$

$$c_i = \frac{(-1)^{i-1}}{3!V}\begin{vmatrix} 1 & x_2 & z_2 \\ 1 & x_3 & z_3 \\ 1 & x_4 & z_4 \end{vmatrix} \tag{3.14}$$

$$d_i = \frac{-(-1)^{i-1}}{3!V}\begin{vmatrix} 1 & x_2 & y_2 \\ 1 & x_3 & y_3 \\ 1 & x_4 & y_4 \end{vmatrix} \tag{3.15}$$

We will use a simple problem to illustrate the basic concept. Consider the problem of computing the perimeter of a circle with radius R.

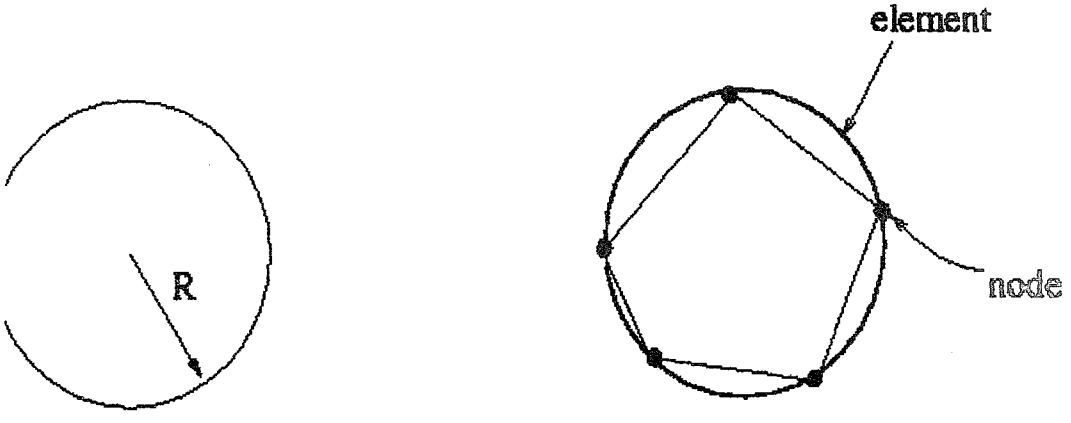

Figure 3.1 Circle discretized into 5 ``elements" and 5 ``nodes"

- Step 1: Finite Element Discretization

Discretize the circle into a "mesh"' of 5 elements and 5 nodes. Elements and nodes will be defined formally later on, but from Figure 3.1 it can be seen that elements are simply pieces of the circle in this case and nodes are the points where they meet.

- Step 2: Local Approximation of Solution

On each element the length is computed. It is assumed that the length of each arc can be approximated by the length of the chord i.e. we approximate the arc using a straight line.

$$h_e = 2R \sin \frac{\theta_e}{2}$$

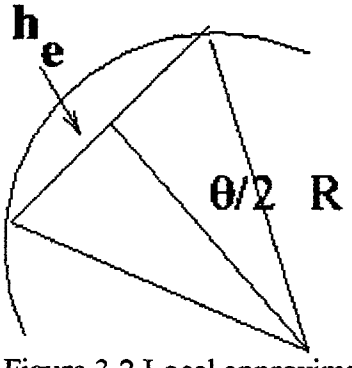

Figure 3.2 Local approximation of arc length on each ``element"

where h_e is the length of each segment, θ_e is the angle subtended at the center by each element. Thus, $\theta_e = \frac{2\pi}{n}$

- Step 3: Assemble the Element Equations

Collect the element equations to get a representation of the whole system.

$$P_n = \sum_{e=1}^{n} h_e$$

$$= \sum_{e=1}^{n} 2R \sin(\theta_e/2)$$

$$= \sum_{e=1}^{n} 2R \sin(\pi/n)$$

$$= 2n\, R \sin(\pi/n)$$

- Step 4: Obtain the Solution

n= 5. Thus,

$$P_n = 2nR \sin(\pi/n)$$

$$= 2 \times 5 \sin(\pi/5) = 5.81\, R$$

- Step 5: Analyze the Solution

Let n= 10 then $P_n = 6.18\ R$

Let n=100 then $P_n = 6.282158\ R$

In the limiting case as $n \to \infty$ $\lim_{n \to \infty} P_n = 2\pi R$

The finite element solution converges to the true solution as the number of elements is increased.

3.2 Agilent HFSS

Agilent HFSS is a software package for electromagnetic modeling of passive, three-dimensional structures. It computes scattering parameter (S-parameter) responses for multiple modes, electric field distributions including far-field antenna radiation patterns, impedance and propagation constants for multiple modes. The package uses Maxwell's equations to solve for electric and magnetic fields and includes dispersion; uses AutoCAD industry-standard interface to handle unrestricted geometries that contain an unlimited number of dielectrics and ports; contains a model parts library; calculates S-parameters and loss values; contains a fast sweep mode for a fast preview of electromagnetic response; provides field plots, graphs and tables; models radiated structures and calculates radiation patterns and related antenna parameters at all angles for detailed antenna performance analysis.

To generate an electromagnetic field solution from which S-parameters can be computed, Agilent HFSS employs the finite element method. In general, the finite element method divides the full problem space into thousands of smaller regions and represents the field in each sub-region (element) with a local function. In Agilent HFSS, the geometric model is automatically divided into a large number of tetrahedra, where a single tetrahedron is formed by four equilateral triangles. This collection of tetrahedra is referred to as the finite element mesh. The value of a vector field quantity (such as the H-field or the E-field) at points inside each tetrahedron is interpolated from the vertices of the tetrahedron. At each vertex, Agilent HFSS stores the components of the field that are tangential to the three edges of the tetrahedron. In addition, the component of the vector field at the midpoint of selected edges that is tangential to a face and normal to

the edge can also be stored. The field inside each tetrahedron is interpolated from these nodal values.

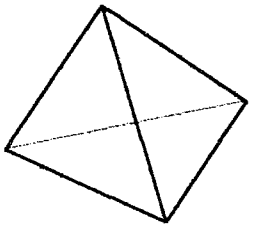

Figure 3.3 A tetrahedron

By representing field quantities in this way, Maxwell's equations can be transformed into matrix equations that are solved using traditional numerical methods.

To calculate the S-matrix associated with a structure, the following steps are performed:

1. The structure is divided into a finite element mesh.

2. The waves on each port of the structure that are supported by a transmission line having the same cross-section as the port are computed.

3. The full electromagnetic field pattern inside the structure is computed, assuming that each of the ports is excited by one of the waves.

The field pattern of a traveling wave inside a waveguide can be determined by solving Maxwell's equations. The following equation is derived directly from Maxwell's equation.

$$\nabla x(\frac{1}{\mu_r} \nabla x\mathbf{E}(x,y,z)) - k_0^2 \varepsilon_r \mathbf{E}(x,y,z) = 0 \qquad (3.16)$$

where:

E(x,y,z) is a complex vector representing an oscillating electric field.

μ_r is the complex relative permeability.

k_0 is the free space phase constant, $\omega\sqrt{\mu_0\varepsilon_0}$

ω is the angular frequency: $2\pi f$.

ε_r is the complex relative permittivity.

The physical electric field, E(x,y,z,t), is the real part of the product of the phasor, E(x,y,z) and e^{jwt} :

$$E(x,y,z,t) = Re[E(x,y,z)\, e^{jwt}] \tag{3.17}$$

4. The generalized S-matrix is computed from the amount of reflection and transmission that occurs.

The final result is an S-matrix that allows the magnitude of transmitted and reflected signals to be computed directly from a given set of input signals, reducing the full three-dimensional electromagnetic behavior of a structure to a set of high frequency circuit values.

There are three variations to the solution process:

1.Adaptive Solution:

An adaptive solution is one in which a finite element mesh is created and automatically refined to increase the accuracy of succeeding adaptive solutions. The adaptive solution is performed at a single frequency. (Often, this is the first step in generating a non-adaptive frequency sweep or a fast frequency sweep.).

2.Non-adaptive Discrete Frequency Sweep:

To perform this type of solution, an existing mesh is used to generate a solution over a range of frequencies. The starting and ending frequency, and the interval at which new solutions are generated will be specified. The same mesh is used for each solution, regardless of the frequency.

3.Non-adaptive Fast Frequency Sweep

This type of solution is similar to a discrete frequency sweep, except that a single field solution is performed at a specified center frequency. From this initial solution, the system employs asymptotic waveform evaluation (AWE) to extrapolate an entire bandwidth of solution information. While solutions can be computed and viewed at any frequency, the solution at the center frequency is the most accurate.

4. MODELING A HUMAN HEAD AND CELLULAR PHONE ANTENNA WITH AGILENT HFSS SOFTWARE

In this chapter, modeling a human head and cellular phone antenna used in simulations is explained and the results are given.

4.1 Multilayered-Spherical Model of a Human Head

Multilayered Spherical Model, which approximates the primate spherical structure irradiated by plane waves in the cellular frequencies range, was used to model a human head by Shapiro in 1971 [37]. Weil extended his work in 1975 to study the effect of hotspot shifts with changes in frequencies [38].

To solve the dosimetry problem caused by electromagnetic radiation on the human body is too complicated. As a result we only model the electromagnetic effects on the human head. Figure 4.1 shows that the basic spherical model with a plane wave, polarized in the x-direction and propagating in the z-direction, incident upon it [38].

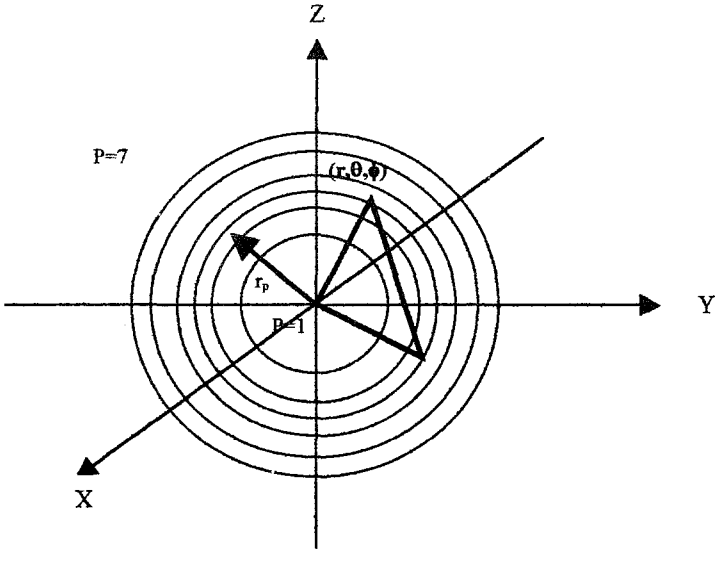

Figure 4.1 Plane wave incident upon spherical model with six concentric shells [38]

The model consists of a core of brain-like material (region 1) surrounded by six concentric layers of different materials. The seventh layer represents the air.

Table 4.1
Tissues and radius used for six concentric shell model [38]

Region (p)	Tissue Modeled	Layer Thickness (cm)	Relative Permittivity ε_r
1	Brain	9.10	60
2	CSF	0.20	76
3	Dura	0.05	45
4	Bone	0.40	8.5
5	Fat	0.15	5.5
6	Skin	0.10	45

The electric fields induced in a sphere or spherical layer of tissue by an incident plane wave field can be calculated from the general vector spherical wave solutions of the wave equation, which is based on Mie Theory and formulated Stratton. Mathematical details have been given by Shapiro et al [37]. The basic solution involves expanding the incident and secondary (scattered and internally induced) fields into vector spherical harmonics. Tangential components of E and H-fields are then equated at the six regional boundaries in order to determine the various unknown expansion coefficients, a^r_n, b^r_n, a^t_n, a^t_n, for each region.

Incident:

$$E_i = E_0 e^{j\omega t} \sum_{n=1}^{\infty} i^n \frac{2n+1}{n(n+1)} \left(m^{(1)}_{oln} - jn^{(1)}_{eln}\right) \tag{4.1}$$

Reflected:

$$E_r = E_0 e^{j\omega t} \sum_{n=1}^{\infty} i^n \frac{2n+1}{n(n+1)} \left(a^r_n m^{(3)}_{oln} - j\, b^r_n n^{(3)}_{eln}\right) \tag{4.2}$$

Induced within sphere:

$$E_t = E_0 e^{j\omega t} \sum_{n=1}^{\infty} i^n \frac{2n+1}{n(n+1)} \left(a^t_n m^{(1)}_{oln} - j\, b^t_n n^{(1)}_{eln}\right) \tag{4.3}$$

Scattering cross section:

$$Q_s = \frac{2\pi}{k^2_2} \sum_{n=1}^{\infty} (2n+1) \left(|a^r_n|^2 + |b^r_n|^2\right) \tag{4.4}$$

Total cross section:

$$Q_t = \frac{2\pi}{k^2_2} \Re \sum_{n=1}^{\infty} (2n+1) \left(a^r_n + b^r_n\right) \tag{4.5}$$

Absorption cross section:

$$Q_a = Q_t - Q_s \tag{4.6}$$

The average density of the power absorbed throughout the model:

$$w_a = 3/(8\pi)\sqrt{\frac{\varepsilon_o}{\mu_o}}\frac{E^2{}_o Q_a}{r^3{}_{N-1}} \tag{4.7}$$

where the function m_{oln} and n_{eln} are defined and the coefficients a_n and b_n are obtained [38].

Although modeling the human head in six layers is more realistic, it is possible to model the human head in single layer [8,15,18,21] or in three layers [15]. In our study, a single layered and three layered spherical models with diameter of 20 cm were used to model a human head and for the single-layered model, the dielectric constant ε_r of the human head was taken as 39.5 and dielectric loss tangent, which is $\varepsilon''/\varepsilon'$, as 0.354, σ as 0.9 and ρ as 1100 [15]. For three-layered model, the following values were used.

Table 4.2

The tissues and the properties used in simulations [15]

Layer	Tissue Modeled	Thickness (cm)	Relative Permittivity ε_r	Conductivity σ ($m\Omega^{-1}/m$)	Density ρ (kg/m^3)	Loss Tangent ($\varepsilon''/\varepsilon'$)
1	Brain	9.10	56.8	0.9	1050	0.387
2	Bone	0.50	12.5	0.11	1200	0.272
3	Skin	0.40	39.5	1	1100	0.354

4.2 Modeling Dipole Antenna

The antenna used in the simulation was modeled as a dipole antenna with a length of 5 cm.

a)

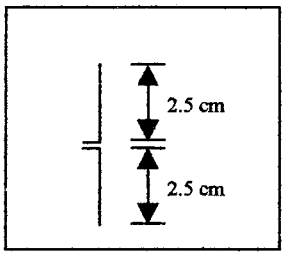

b)

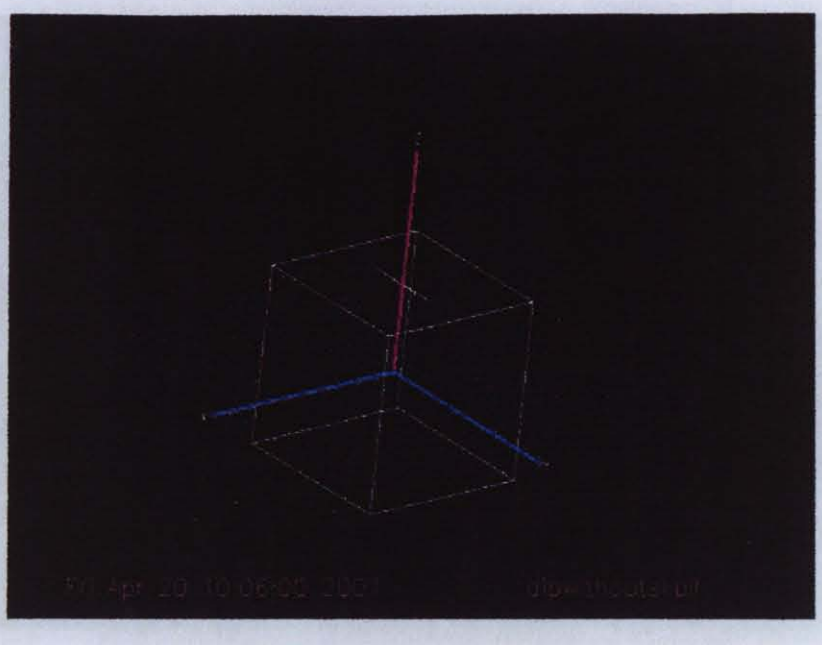

Figure 4.2 a) The antenna model used in study
b) The location of the antenna

The voltage source was located in the center gap of the dipole antenna. The output power was 1W.

The location of the antenna with the human head was as follows:

a)

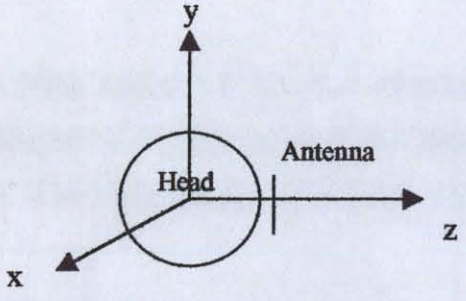

b)

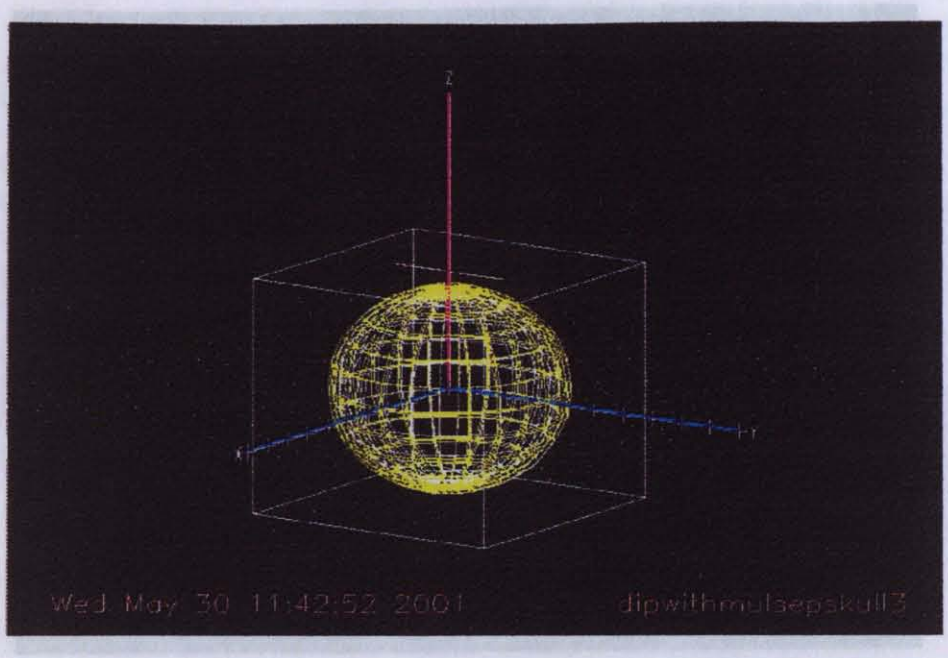

Figure 4.3 a) Geometry of the equivalent dipole antenna and human head
b) The model drawn in HFSS software package

The distance between head and antenna was 1.45 cm.

4.3 Simulation

The Agilent HFSS (High Frequency Structure Simulator) program that was used to calculate the full three-dimensional electromagnetic field inside the structure was based on the finite element method. The finite element mesh that was created for the structure is shown in Fig.4.4.

The accuracy of the solution depends on how small each of the individual elements (tetrahedra) is. It was possible to refine the mesh size in the program. But, generating a field solution for meshes with a large number of elements required a significant amount of computing power and memory. Therefore, a mesh size enough to obtain an accurate field solution was advisable so, the minimum length of each edge of tetrahedra in the structure was 0.2 cm. In most previous studies, the iteration distance was taken as 0.5 cm.

Figure 4.4 Finite Element Mesh

The solution was performed at a single frequency of 900 MHz.

Agilent HFSS imposes boundary conditions on all surfaces exposed to the edge of the meshed problem region. This includes all outer surfaces and all surfaces exposed to voids and surface discontinuities within the structure. The radiation boundary condition, which encloses the whole structure, was selected in our problem. Radiation boundary models surfaces that represent open surfaces. Energy is allowed to radiate from these boundaries instead of being contained within them; waves can radiate out of the structure and toward the radiation boundary. The system absorbs the wave at the radiation boundary, essentially ballooning the boundary infinitely further away from the structure and into the space. The tangential component of the E-field was soluted by the program. In our problem, the radiation boundary was a cube with a length of 23 cm. The material was assigned to the radiation boundary as air.

4.4 SAR Computation

It was possible to view and analyze the E and H fields, far fields, and antenna parameters by the post processor of the program.

The E-field data could be contained in a file. The format of this file was as follows:

T# (tetrahedron1,2,3,.....)

Vertex 1 (x,y,z)
Vertex 1 (x,y,z)
Vertex 1 (x,y,z)
Vertex 1 (x,y,z)
Data at vertex 1 : (vector x (re,im), y (re,im), z (re,im))
Data at (V1+V2)/2 : (vector x (re,im), y (re,im), z (re,im))
Data at (V1+V3)/2 : (vector x (re,im), y (re,im), z (re,im))
Data at (V1+V4)/2 : (vector x (re,im), y (re,im), z (re,im))
Data at vertex 2 : (vector x (re,im), y (re,im), z (re,im))
Data at (V2+V3)/2 : (vector x (re,im), y (re,im), z (re,im))
Data at (V2+V4)/2 : (vector x (re,im), y (re,im), z (re,im))
Data at vertex 3 : (vector x (re,im), y (re,im), z (re,im))
Data at (V3+V4)/2 : (vector x (re,im), y (re,im), z (re,im))
Data at vertex 4 : (vector x (re,im), y (re,im), z (re,im))

A program was written in C++ to read these data, to find the middle point of each tetrahedron and to take the average of magnitudes of E-field at vertices and to apply these data to the SAR formula (see Appendix).

4.5 Simulation Results

4.5.1 The Dipole Antenna

The antenna parameters, which were calculated by the simulation program, were listed below:

Table 4.3
Antenna Parameters

Power radiated (W)	0.5026069761	
Effective angle (degrees)	429.20	
Directivity (dB)	2.246773142	
Gain (dB)	-0.7409417352	
,Maximum intensity (W/Steradian)	0.06709589687	
Angle of U max (theta,phi)	75.00	0
E(theta) max (mag,phase)	0.1642726371	-1208455229
E(phi) max (mag,phase)	7.108244375	148.378144
E(x) max (mag,phase)	0.04251688708	-120.8455229
E(y) max (mag,phase)	7.108244375	148.378144
E(z) max (mag,phase)	0.1586751828	59.15447714

The electric far field, which was calculated by 4 x π x U_{max} where U_{max} was the maximum radiation intensity in W/Steradian, is shown in Fig. 4.5.

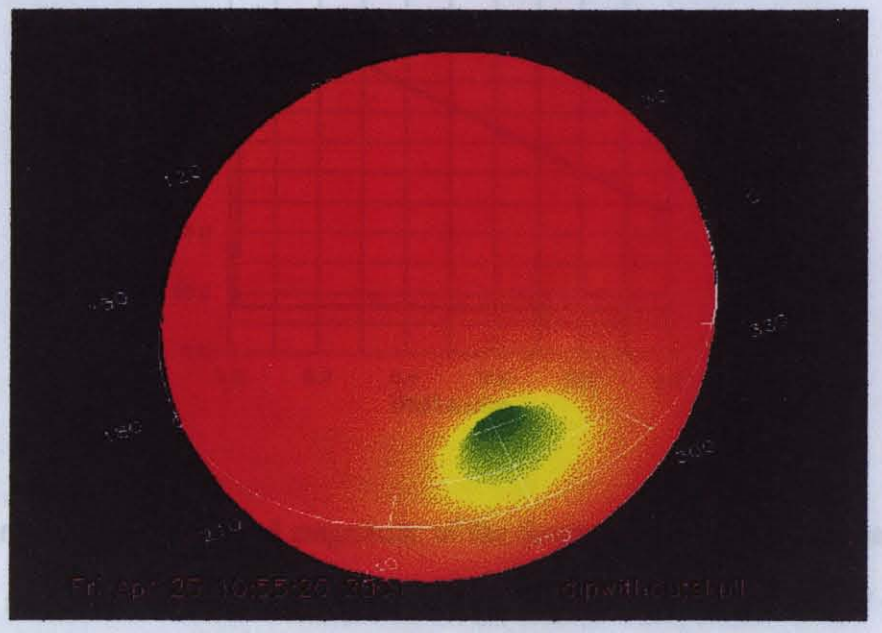

Figure 4.5 The far field of the antenna (without human head)

The three-dimensional radiation intensity pattern of the antenna in Fig.4.5 was obtained as indicated in the literature [39].

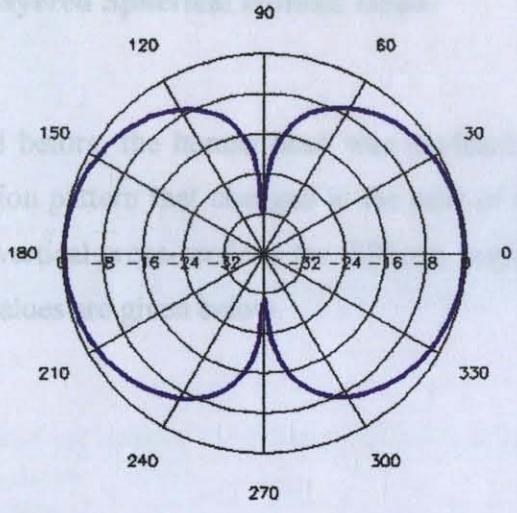

Figure 4.6 The horizontal cut of the far field

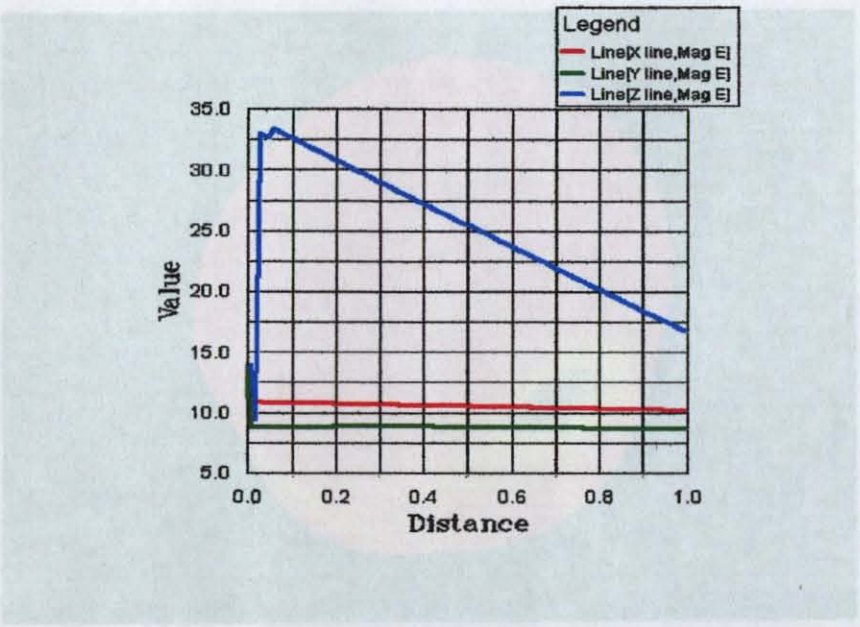

Figure 4.7 The normalized magnitude of the electric field (V/m) along the axes.

The magnitude of E was a scalar field representing the magnitude of the electric field at each point in the problem space, represented by:

$$\sqrt{\Re\,[E_x^{j\omega t}]^2 + \Re\,[E_y^{j\omega t}]^2 + \Re\,[E_z^{j\omega t}]^2} \qquad (4.8)$$

4.5.2 The Single-Layered Spherical Human Head

As indicated before, the human head was modeled in a single layer with the same antenna. The radiation pattern that changed in the case of the presence of the human head, the horizontal and vertical cross-sections for different angles, the magnitude of the electric field and the SAR values are given below.

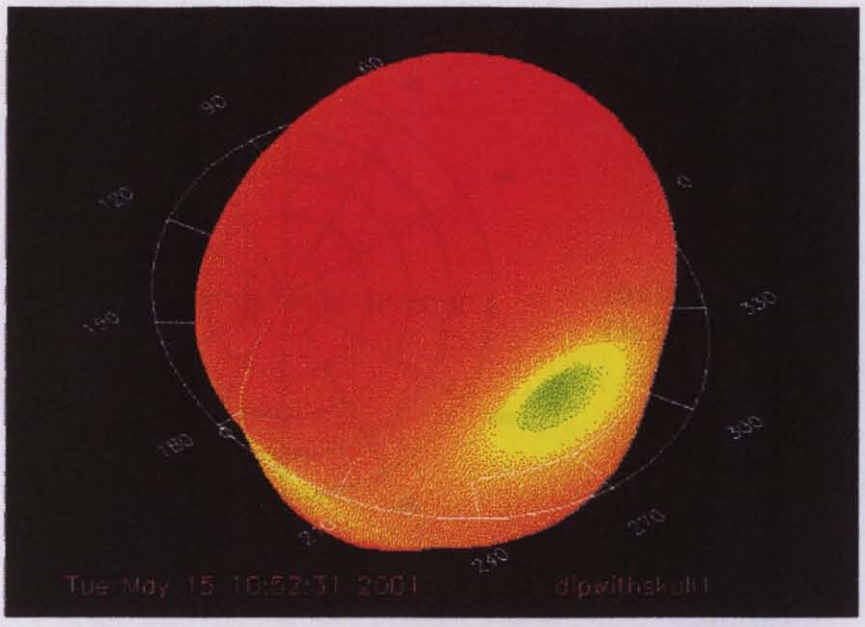

a)

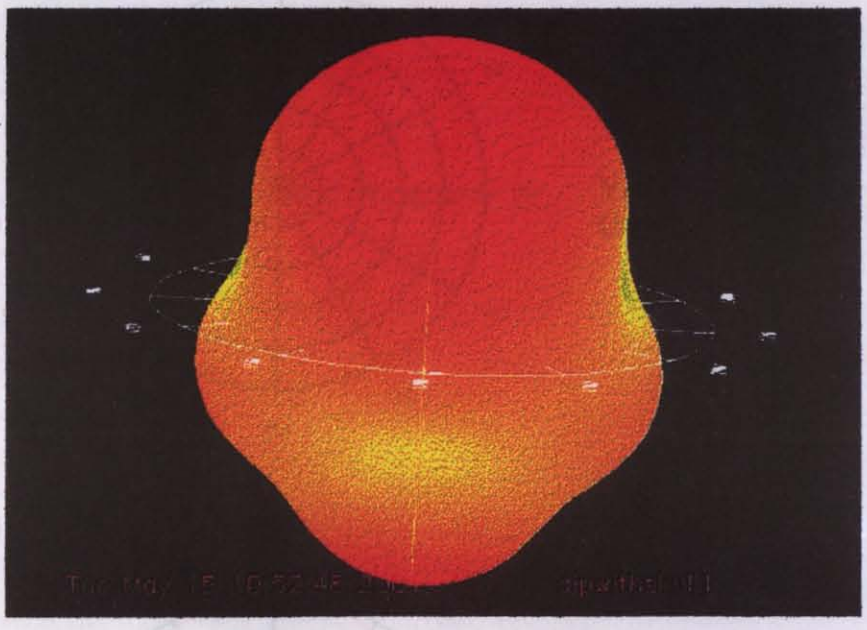

b)

Figure 4.8 The far field patterns of the antenna with the single-layered human head model
a) From above
b) From side

In Fig. 4.9, the 2-dimensional cross-section patterns of the far field are given.

a)

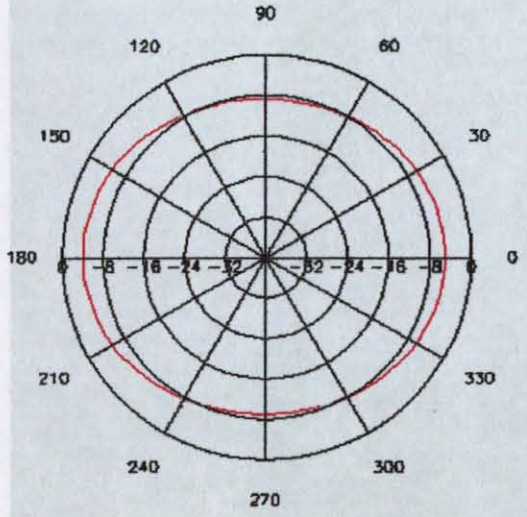

Horizontal cut, 90°
On XY-plane

b)

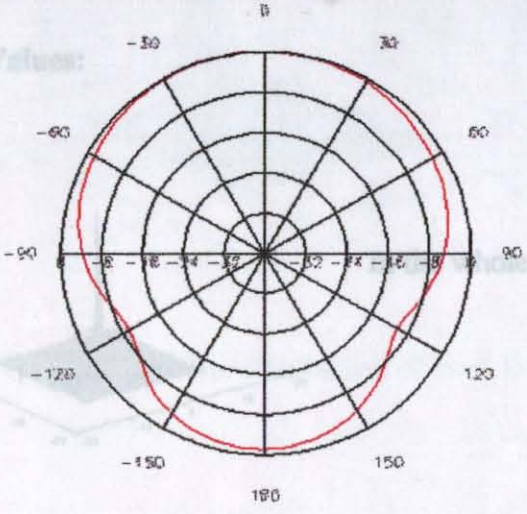

Vertical cut, 180°
On YZ-plane

c)

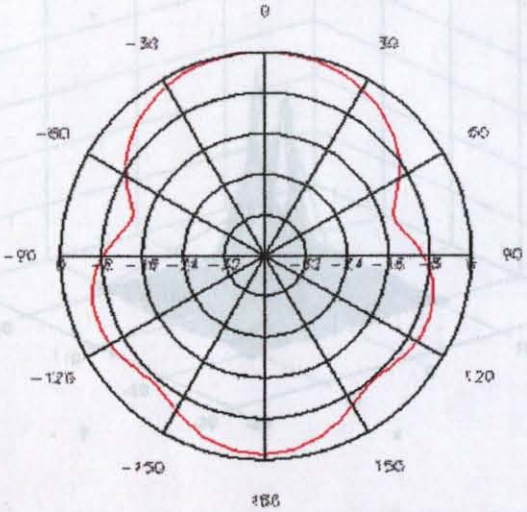

Vertical cut, 90°
On YZ-plane

Figure 4.9 The 2D cross-section patterns of the far field

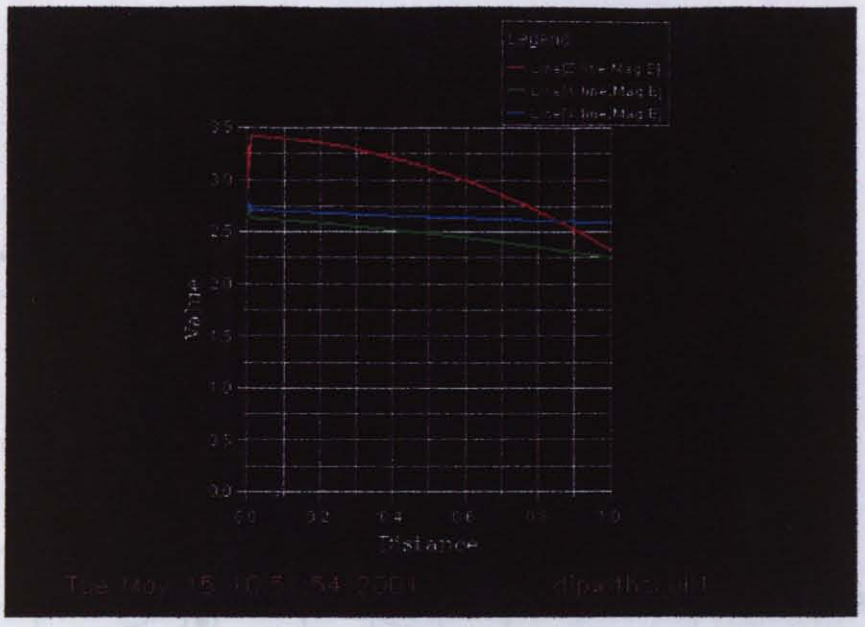

Figure 4.10 The normalized magnitude of the electric field (V/m) along the axes.

The SAR Values:

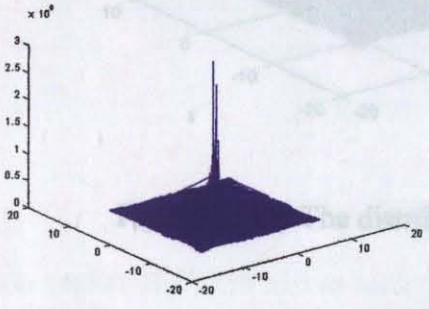

In the whole model

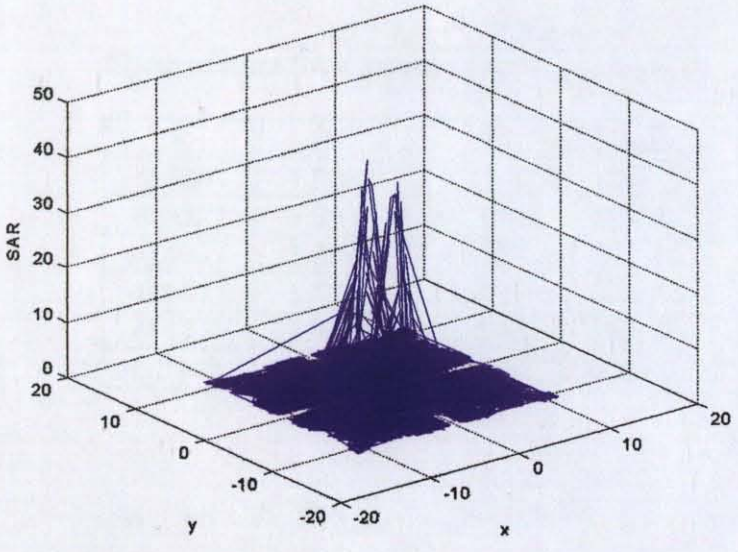

In the sphere

Figure 4.11a) The distribution of local SAR values in the XY-plane.

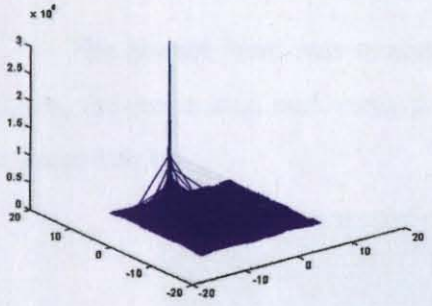

In the whole model

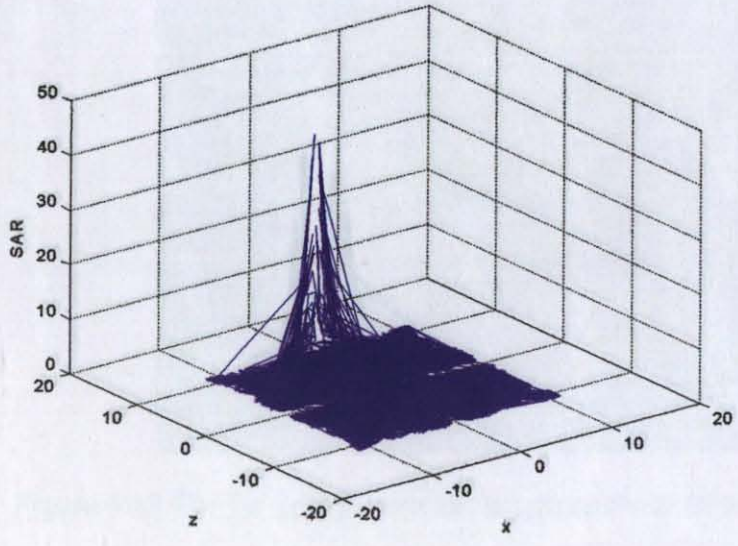

In the sphere

Figure 4.11b) The distribution of local SAR values in the XZ-plane.

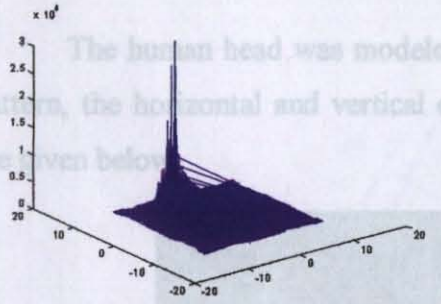

In the whole model

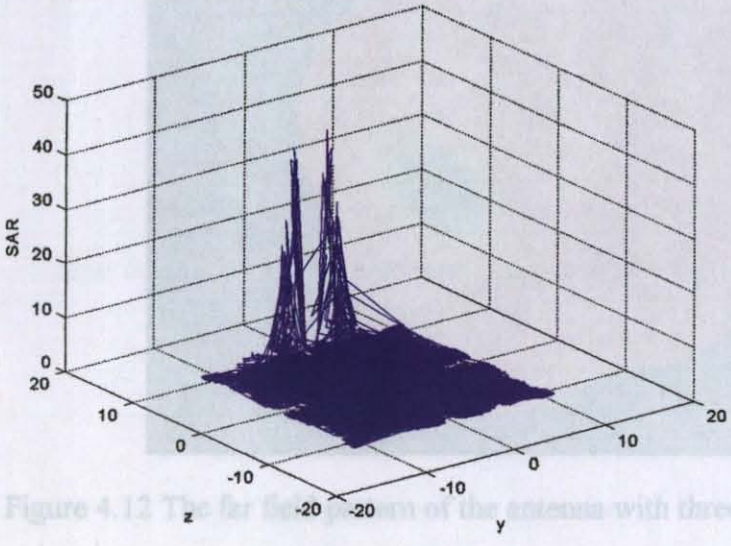

In the sphere

Figure 4.11c) The distribution of local SAR values in the YZ-plane.

In the region of –10 to +10 at each plane, some of the local SAR values were listed below:

Table 4.4
Some of local SAR values in the single-layered spherical human head

X	Y	Z	Depth	Local SAR
-0.1241	1.8982	9.9540	0.0460	40.7296 (Max)
-0.4527	1.9938	9.9054	0.0946	36.2210
-0.4527	2.2095	9.8770	0.1230	35.4222
-0.6087	1.4978	9.9621	0.0379	29.8588
-0.4737	2.9492	9.7644	0.2356	22.5616
0.2542	-3.0786	9.7228	0.2772	20.5131

4.5.3 The Three-Layered Spherical Human Head

The human head was modeled in three layers with the same antenna. The radiation pattern, the horizontal and vertical cross-sections for different angles and the SAR values are given below.

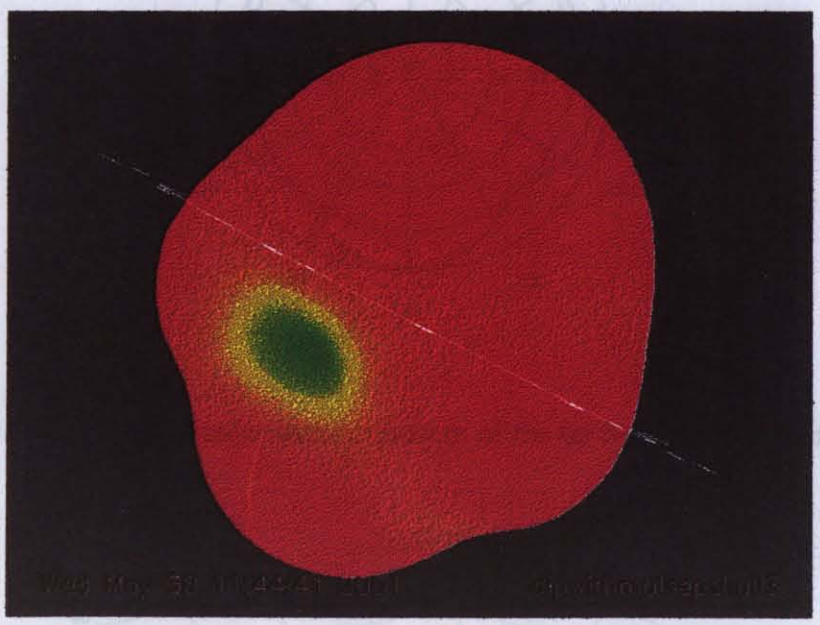

Figure 4.12 The far field pattern of the antenna with three-layered human head model

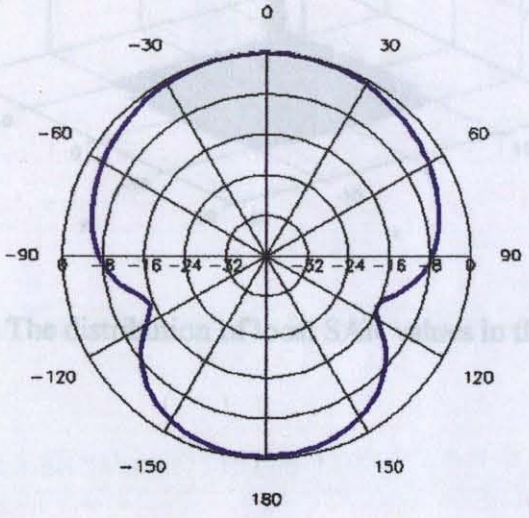

Figure 4.13a) The 2D cross-section pattern of the far field (Vertical cut, 180°)

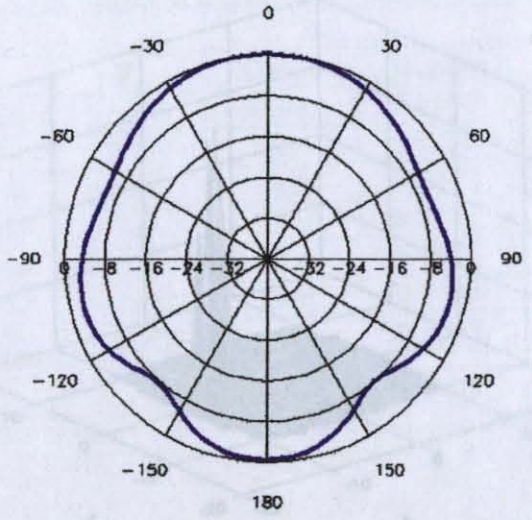

Figure 4.13b) The 2D cross-section pattern of the far field (Vertical cut, 90°)

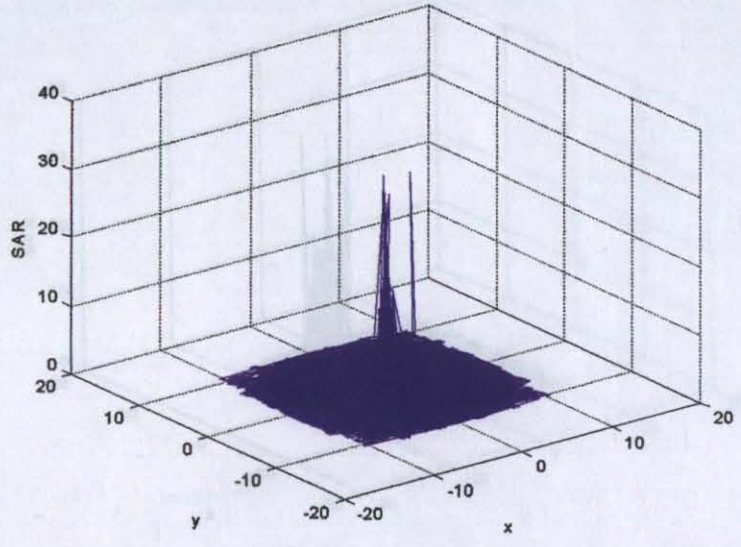

Figure 4.14a) The distribution of local SAR values in the XY-plane.

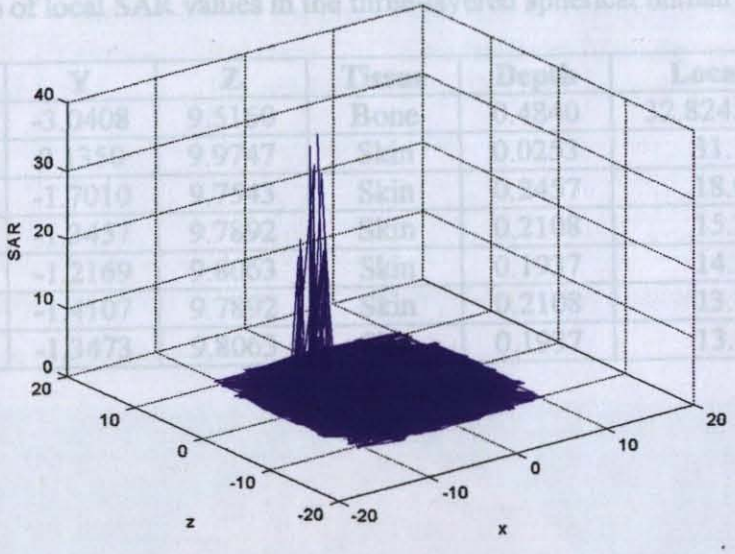

Figure 4.14b) The distribution of local SAR values in the XZ-plane.

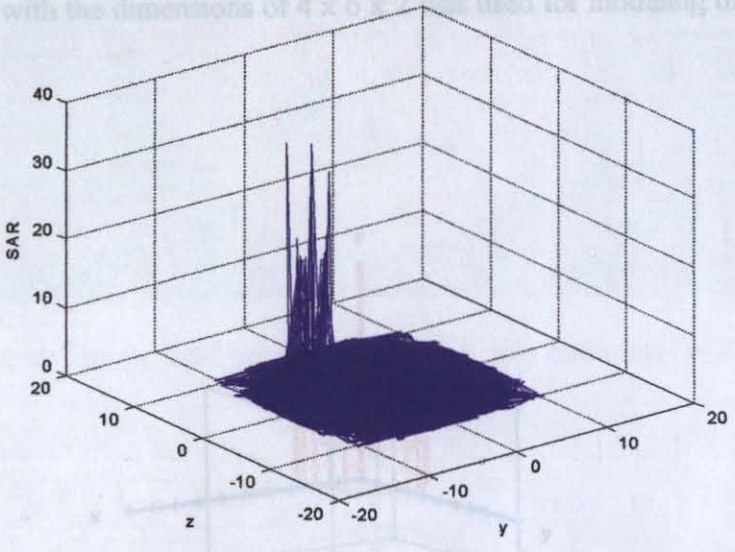

Figure 4.14c) The distribution of local SAR values in the YZ-plane.

Some of the local SAR values in the sphere of –10 to +10 were listed below:

Table 4.5
Some of local SAR values in the three-layered spherical human head

X	Y	Z	Tissue	Depth	Local SAR
0.4333	-3.0408	9.5160	Bone	0.4840	32.8245 (Max.)
-0.1329	0.1350	9.9747	Skin	0.0253	31.1396
-1.3992	-1.7010	9.7543	Skin	0.2457	18.0715
-1.4107	-1.3457	9.7892	Skin	0.2108	15.3930
-1.3473	-1.2169	9.8063	Skin	0.1937	14.1395
-1.3457	-1.4107	9.7892	Skin	0.2108	13.9453
-1.2169	-1.3473	9.8063	Skin	0.1937	13.4591

4.5.4 The Three-Layered Ellipsoid Rat Model

Ellipsoid with the dimensions of 4 x 6 x 2 was used for modeling of the head of rat.

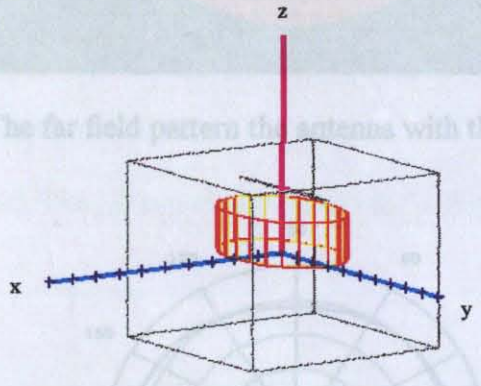

Figure 4.15 The model of the head of the rat and the antenna

The relative permittivity ε′, conductivity σ, and density ρ used in simulation are given in Table 4.6. The antenna and the rat model were in a radiation boundary, which was modeled as a cube with a length of 8 cm. The output power was 2 W.

Table 4.6
The tissues and the properties used in simulations [40]

Layer	Tissue Modeled	Thickness (cm)	Relative Permittivity ε_r	Conductivity σ (mΩ^{-1}/m)	Density ρ (kg/m^3)	Loss Tangent ($\varepsilon''/\varepsilon'$)
1	Brain	1.91	55	1	1050	0.363
2	Bone	0.05	5.5	0.15	1990	0.6
3	Skin	0.04	45	0.76	1040	0.337

The far-field radiation pattern and 2D cross-sectional images and the local SAR values in the planes are given below:

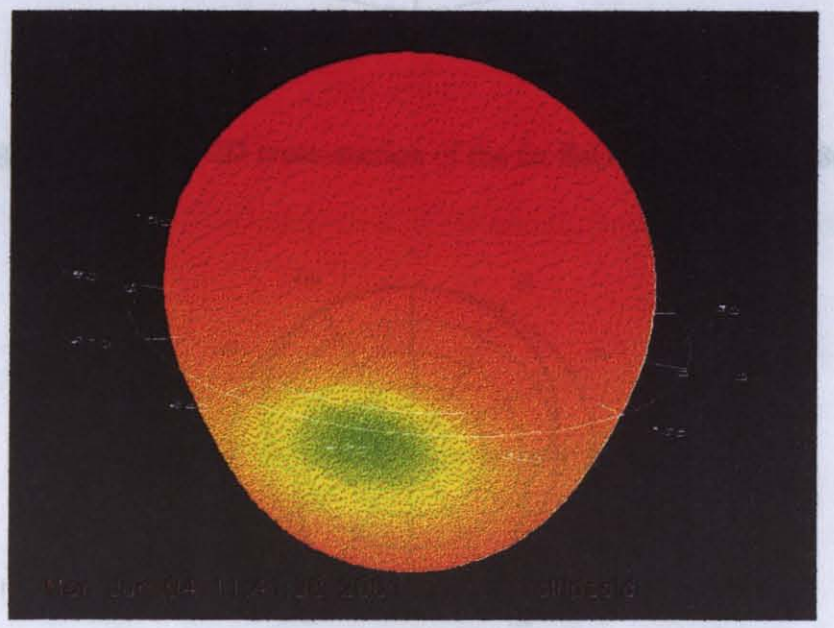

Figure 4.16 The far field pattern the antenna with three-layered rat model

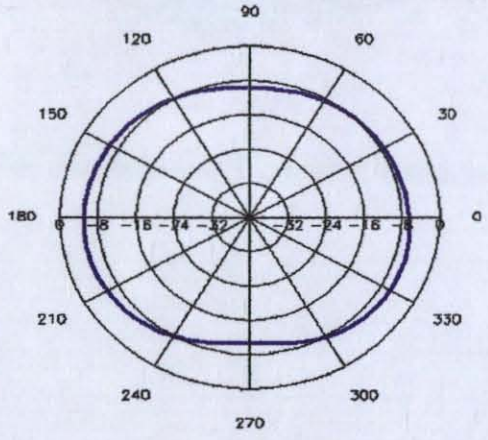

Figure 4.17a) The 2D cross-section pattern of the far field (Horizontal cut, 90)

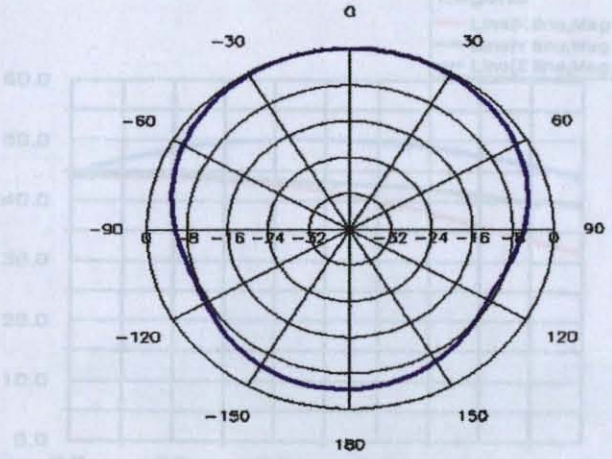

Figure 4.17b) The 2D cross-section of the far field (Vertical cut, 180)

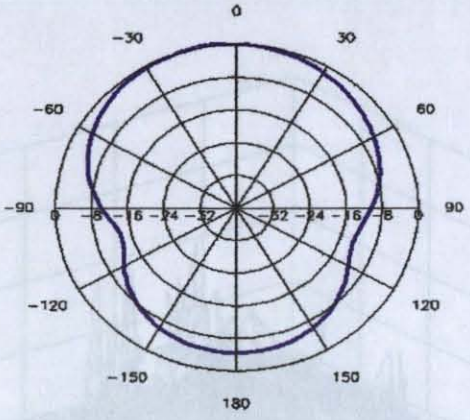

Figure 4.17c) The 2D cross-section of the far field (Vertical cut, 90)

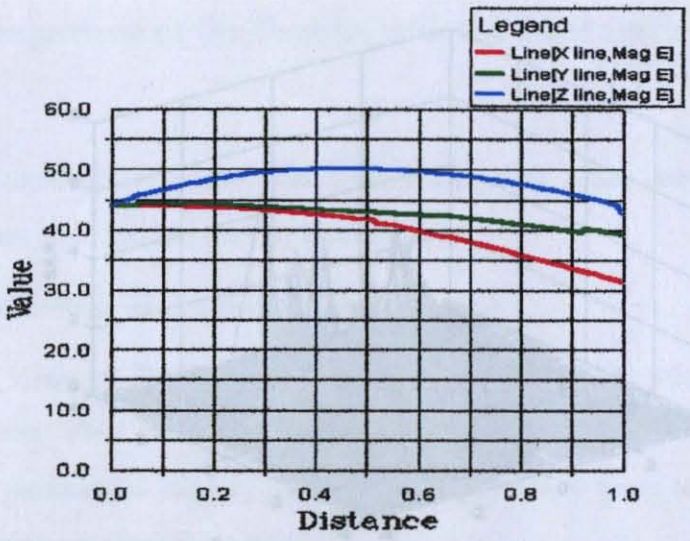

Figure 4.18 The normalized magnitude of the electric field (V/m) along the axes.

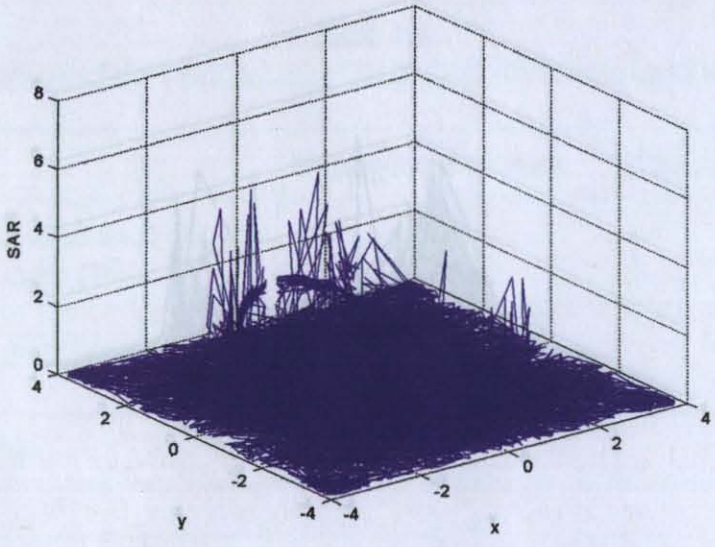

Figure 4.19a) The distribution of local SAR values in the XY-plane.

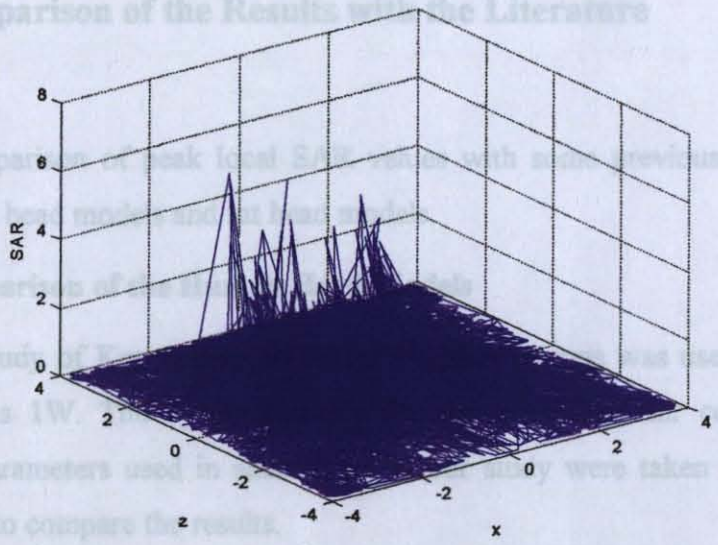

Figure 4.19b) The local SAR values in the XZ-plane.

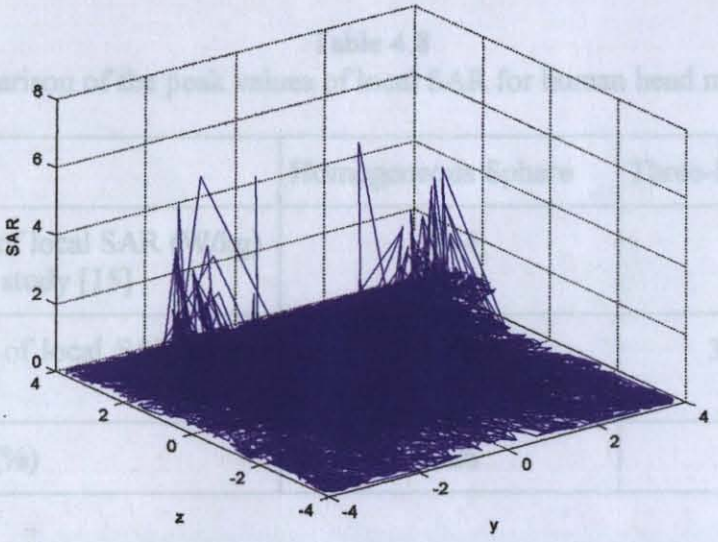

Figure 4.19c) The local SAR values in the YZ-plane.

Table 4.7
Some of local SAR values in the three-layered ellipsoid rat-head model

X	Y	Z	Tissue	Depth	Local SAR
-1.7119	-2.2760	1.9869	Skin	0.0131	6.0422 (Max.)
-1.8129	1.1332	1.8463	Brain	0.1537	5.9076
-0.5135	-2.8664	1.8463	Brain	0.1537	5.4977
1.0917	2.9789	1.8138	Brain	0.1862	4.5635
-1.0917	-2.9789	1.8138	Brain	0.1862	4.2586
-1.7563	-2.1891	1.9101	Bone	0.0899	4.0053

4.6 The Comparison of the Results with the Literature

The comparison of peak local SAR values with some previous studies are given below for human head models and rat head models.

4.6.1 The Comparison of the Human Head Models

In the study of Konstantina S. Nikita a dipole antenna was used and the antenna input power was 1W. The dyadic Green's function was used for computation of the problem. The parameters used in simulations in our study were taken from this study in order to be able to compare the results.

The peak values of local SAR in Nikita's study [15] and in our study were given in Table 4.8. The difference between two studies is as follows:

Table 4.8
Comparison of the peak values of local SAR for human head modeling

	Homogeneous Sphere	Three-Layer Sphere
Peak value of local SAR (W/kg) of Nikita' s study [15]	39.4	29.3
Peak value of local SAR of our study	40.7296	32.8245
Difference (%)	3.26	10.73

The radiation pattern obtained by Nikita was as follows:

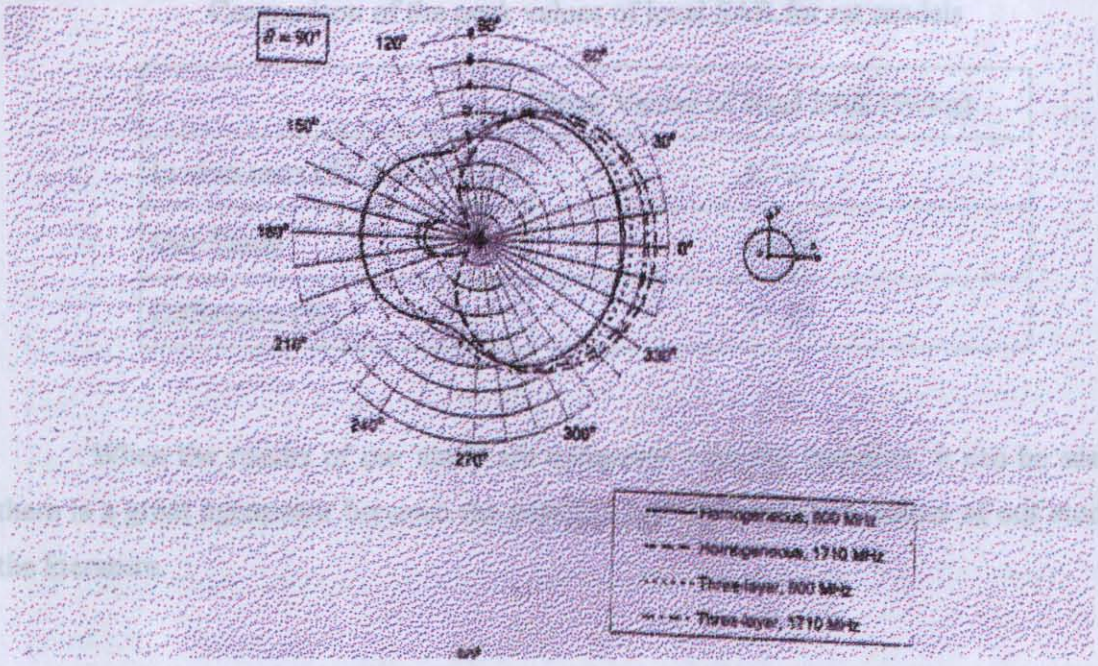

a)

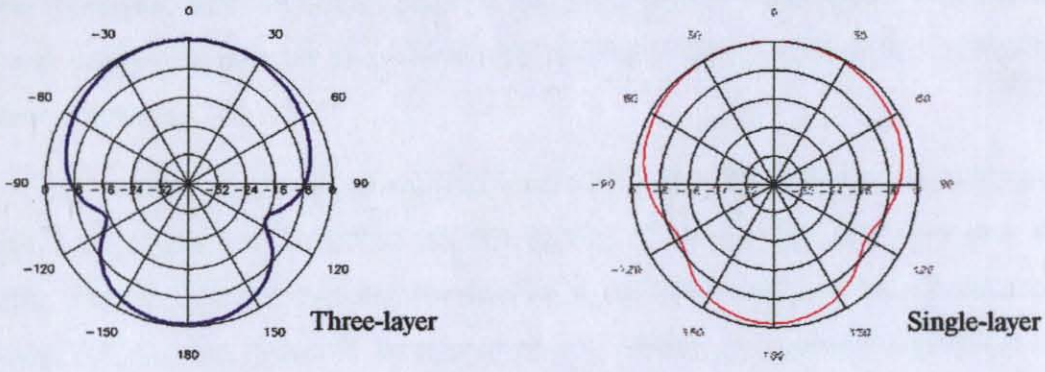

b)

Figure 4.20 a) Radiation pattern obtained by Nikita [15]
b) Radiation patterns obtained in our study

4.6.2 The Comparison of the Rat Models

The results of the rat-head model were compared with the results of **in vivo** tests, which were conducted on the rats at Istanbul University, Cerrahpasa Faculty of Medicine [41]. The in vivo tests were repeated with different E-field values; for the comparison, the result of 51.5 V/m of E-field, which was the maximum E-field value in our simulation, was taken into consideration. The output power in our simulation was 2 W as well as in the in vivo tests.

Table 4.9
Comparison of the peak values of local SAR for rat models

	Peak Values of local SAR (W/kg)
In vivo tests (51.5 V/m) [41]	6.732
Our Study	6.042
Difference (%)	11.42

When the results of our study are compared with the literature, it can be seen that there is a great agreement between the patterns and the local SAR values of our study and the literature.

5. CONCLUSION

In this study, spherical human heads and dipole antenna were modeled to investigate the effects of the electromagnetic field of an antenna on a human head because of the impossibility of doing in vivo experiments on humans. The Finite Element Method supported by a C++ program was used to calculate the local SAR values, which represent the biological effects of EM radiation. Local SAR values were calculated for two different human head models (single and three-layered spherical models) and for three-layered rat head models.

The application presented here, apart from constituting a worst-case approximation for the radiation hazards, seems to be reliable when comparing the results with the literature.

Future research in this subject might be to investigate the SAR with different antenna types and different output powers, the interaction of base station with the human body and finally it is possible to prove Kronig-Kramers' relationship using this method by a reverse approach.

The pattern of energy absorption inside an irradiated body is non-uniform, and biological responses are dependent on distribution of energy and the body part that is affected. The rate of absorption and the distribution of EMR energy in an organism depend on many factors: the dielectric composition (i.e., ability to conduct electricity) of the irradiated tissue, e.g., bones, with a lower water content, absorb less of the energy than muscles; the size of the object relative to the wavelength of the EMR (thus, the frequency); shape, geometry, and orientation of the object; and configuration of the radiation. The biological and health consequences of these exposure conditions need further understanding. So, another question appears: whether the SAR values determined by the Health Organizations are safe enough. The standards are being lowered from time to time. After learning the exact biological responses, the SAR values can be determined properly.

APPENDIX : THE FLOWCHART OF THE C++ PROGRAM

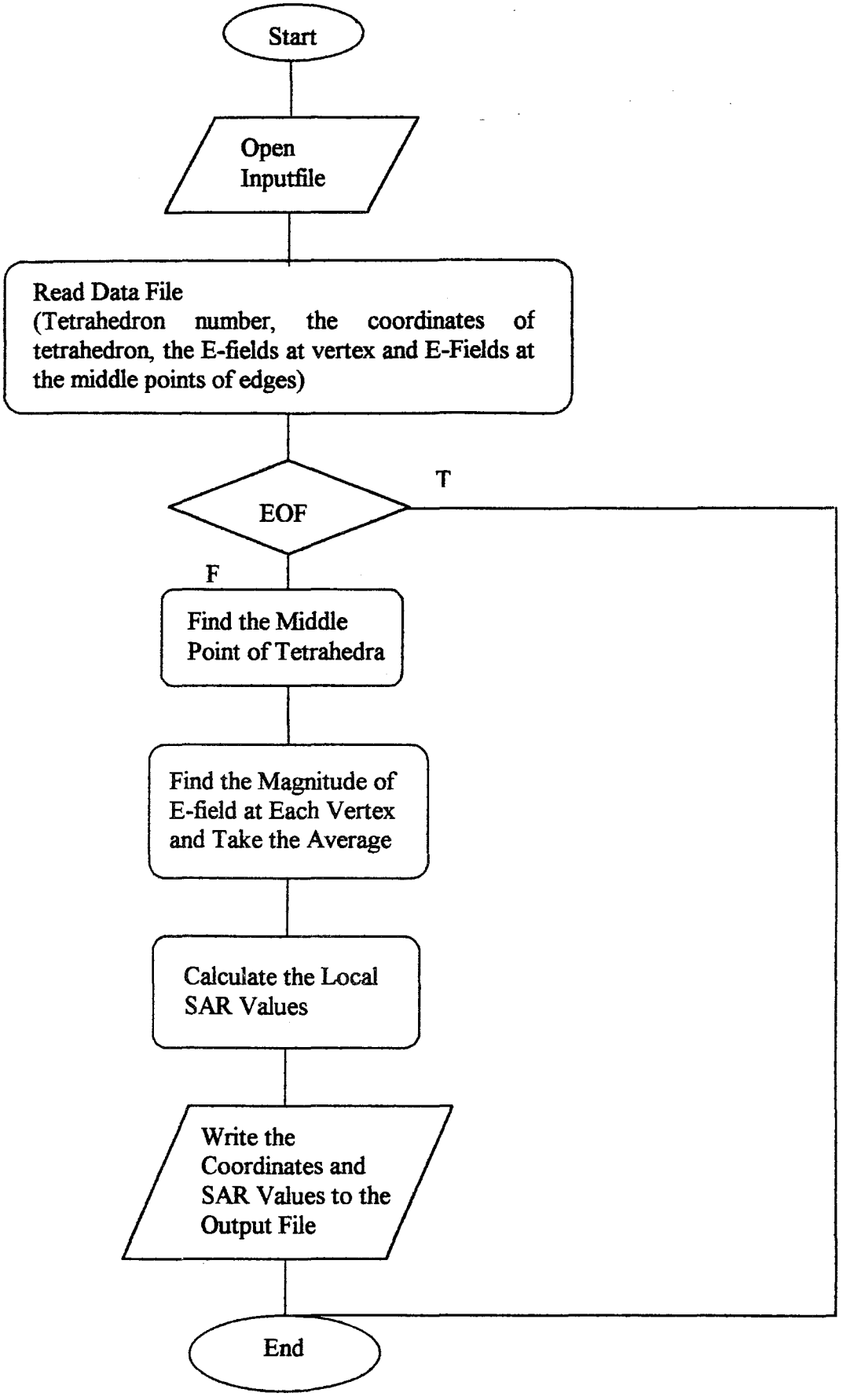

REFERENCES

1. Bernardi, P., S. Pisa, E. Puizzi, "Specific Absorption Rate and Temperature Increases in the Head of a Cellular-Phone User," *IEEE Transactions on Microwave Theory and Techniques*, Vol. 48, no. 7, pp. 1118-1126, July 2000.
2. Hagmann, M.J., O.P. Gandhi and C.H. Durney, "Numerical Calculation of Electromagnetic Energy Deposition for a Realistic Model of Man," *IEEE Transactions on Microwave Theory and Techniques*, Vol. 27, pp. 804-809, 1979.
3. Mitch, A.R., D.F. Hriffiths, *The Finite Difference Method in Partial Differential Equations*, John Wiley and Sons, Chichester, 1980.
4. Arthur, W.G., "Specific Absorption Rates of Energy in Man Models Exposed to Cellular UHF Mobile-Antenna Fields," *IEEE Transactions on Microwave Theory and Techniques*, Vol. MTT-34, no.6, pp. 671-680, 1986.
5. ANSI, "American National Standard Safety Levels With Respect to Human Exposure to Radio Frequency Electromagnetic Fields, 300 kHz to 100 GHz," IEEE, 1982.
6. Balzano, Q., O. Garay, F.R. Stell, " Energy Deposition in Simulated Human Operators of 800-MHz Portable Transmitters," *IEEE Transactions on Vehicular Technology*, Vol. VT.27, no. 4, pp. 174-181, November 1978.
7. Macfarlane, I.R., "Magnitudes of the Near E-Field Close to Hand-Held GSM Digital Mobile Telephones," *A.T.R.*, Vol. 28, no. 2, pp. 61-71, 1994.
8. Toftgard, J., S.N. Hornsleth, "Effects on Portable Antennas of the Presence of a Person," *IEEE Transactions on Antennas and Propagation*, Vol. 41, no. 6, pp. 739-746, June 1993.
9. Chen, H.Y., "Current and SAR Induced in a Human Head Model by the Electromagnetic Fields Irradiated from a Cellular Phone," *IEEE Transactions on Microwave Theory and Techniques*, Vol. MTT-42, no.12, pp. 2249-2254, 1996.
10. Lu, Y., J. Ying, T. Tan, K. Arichandran, "Electromagnetic and Thermal Simulations of 3-D Human Head Model under RF Radiation by Using FDTD and FD Approaches," *IEEE Transactions on Magnetics*, Vol. 32, no.3, pp. 1653-1657, May 1996.

11. Li, L.W., M.S. Leong, P.S. Kooi, T.S. Yeo, "Specific Absorption Rates in Human Head due to Hand Set Antennas: A Comparative Study Using FDTD Method," *Journal of Electromagnetic Waves and Applications*, Vol. 14, pp. 987-1000, 2000.

12. Wang, J. and O. Fujiwara, "The Role of Head Tissue Complexity in the Peak SAR Assessment for Mobile Phones," *Proceedings of the International Wroclaw Symposium on Electromagnetic Compatibility*, June 23-25,2000, pp. 255-259, Wraclow, Poland, 2000.

13. Drossos, A., "The Dependence of Electromagnetic Energy Absorption upon Human Head Tissue Composition in the Frequency Range of 300-3000 MHz," *IEEE Transactions on Microwave Theory and Techniques*, Vol. 48, no.11, pp. 1988-1995, November 2000.

14. Schivoni, A., P. Bertotto, G. Richiardi, and P. Bielli, "SAR Generated by Commercial Cellular Phones-Phone Modeling, Head Modeling, and Measurements," *IEEE Transactions on Microwave Theory and Techniques*, Vol. 48, no.11, pp. 2064-2071, November 2000.

15. Nikita, K.S., G.S. Stamatakos, N.K. Uzunoğlu, and A. Karafotias, "Analysis of the Interaction Between a Layered Spherical Human Head Model and a Finite-Length Dipole," *IEEE Transactions on Microwave Theory and Techniques*, Vol. 48, no.11, pp. 2003-2012, November 2000.

16. Iskander, M.J., Z. Yun and R.Q. Illera, "Polarization and Human Body Effects on the Microwave Absorption in a Human Head Exposed to Radiation from Handheld Devices," *IEEE Transactions on Microwave Theory and Techniques*, Vol. 48, no.11, pp. 1979-1986, November 2000.

17. Mason, P.A., W.D. Hurt, T.J. Walters, J.A. D'Andra, P. Gajšek, K.L. Ryan, D.A. Nelson, K.I. Smith, and J.M. Ziriax, "Effects of Frequency, Permittivity, and Voxel Size on Predicted Absorption Rate Values in Biological Tissue During Electromagnetic-Field Exposure," *IEEE Transactions on Microwave Theory and Techniques*, Vol. 48, no.11, pp. 2050-2057, November 2000.

18. Stevens, N., and L.Martens, "Comparison of Averaging Procedure for SAR Distribution at 900 and 1800 MHz," *IEEE Transactions on Microwave Theory and Techniques*, Vol. 48, no.11, pp. 2180-2184, November 2000.

19. Okana, Y., K. Ito, I. Ida, M. Takahashi, "The SAR Evaluation Method by a Combination of Thermographic Experiments and Biological Tissue-Equivalent Phantoms," *IEEE Transactions on Microwave Theory and Techniques*, Vol. 48, no.11, pp. 2094-2102, November 2000.

20. Lazzi, G., O.P. Gandhi, D.M. Sullivan, "Use of PML Absorbing Layers for the Truncation of the Head in Cellular Telephone Simulations," *IEEE Transactions on Microwave Theory and Techniques*, Vol. 48, no.11, pp. 3033-2039, November 2000.

21. Mangoud, M.A., R.A. AbdAlhameed and P.S. Excell, " Simulation of Human Interaction with Mobile Telephones Using Hybrid Techniques over Coupled Domains" *IEEE Transactions on Microwave Theory and Techniques*, Vol. 48, no.11, pp. 2014-2021, November 2000.

22. Noyes, W.S., T.V. McCaffrey, D.A. Fabry, M.S. Robinette, V.J. Suman, "Effects of Temperature Elevation on Rabbit Cochlear Function: Measured by Distortion-Product Otoacustic Emissions," *Otolaryngology Head Neck Surgery*, Vol. 115(6), pp. 548-552, December 1996.

23. Keck, W., J. Thoma, " Conduction of Thermal Stimuli in the Human Temporal Bone," *Archives of Otolaryngology*, Vol. 245(6), pp. 335-339, 1988

24. International Committee on Non-Ionizing Radiation Protection (ICNIRP), "Guidelines for Limiting Exposure to Time-Varying Electric, Magnetic, and Electromagnetic Fields (up to 300 GHz)," *Health Physics*, Vol. 74, no. 4, pp. 494-522, April 1998.

25. European Council of Health Ministers, "Recommendation of 12 July 1999 on the Limitation of Exposure of the General Public to Electromagnetic Fields (0 to 300 GHz)," *Official Journal of the European Communities*, L.199/59-61, July 1999.

26. European Prestandard, Human Exposure to Electromagnetic Fields, Low-frequency (0 to 10 kHz), European Committee for Electrotechnical Standardization (CENELEC), ENV 50166-1, January 1995.

27. European Prestandard, Human Exposure to Electromagnetic Fields, Low-frequency (10 kHz to 300 GHz), European Committee for Electrotechnical Standardization (CENELEC), ENV 50166-2, January 1995.

28. European Specification, Considerations for the Evaluation of Human Exposure to Electromagnetic Fields (EMFs) from Mobile Telecommunication Equipment (MTE) in the Frequency Range 30 MHz – 6 GHz, European Committee for Electrotechnical Standardization (CENELEC), ES 59005, October 1998.

29. Foster, R.F., and J.E. Moulder, "Are Mobile Phones Safe," *The Spectrum*, Vol. 0018-9235, pp. 23-27, August 2000.

30. Schwan, H.P., "*Dielectric Properties of Biological Materials and Interaction of Microwave Fields at the Cellular and Molecular Level*," in S. M. Michaelson and M. W. Miller (Eds.), *Fundamental and Applied Aspects of Nonionizing Radiation*, pp. 68-75, New York: Plenton Publishing Co., 1975.

31. Takashima, S., and H.P. Schwan, "Passive Electrical Properties of Squid Axon Membrane," *Journal of Membrane Biology*, Vol.17,pp. 51-58, 1974.

32. Fricke, H., "The Electric Capacity of Cell Suspensions," *Phys Rev*, Vol. 21, pp. 708-709, 1923.

33. Cole, K.S., *Membranes, Ions and Impulses*, University of California Press, Berkeley, 1972.

34. Schwan, H.P., "Electrical Properties of Tissues and Cell Suspensions," *Adv Biol Med Phys*, Vol. 5, pp.147-209, 1957.

35. Schwan, H.P., and K.R. Foster, "RF-field Interactions with Biological Systems: Electrical Properties and Biophysical Mechanisms," *Proceedings of IEEE*, Vol. 68(l), pp. 104-113, 1980.

36. Gerald, C.F., P.O. Wheatley, *Applied Numerical Analysis*, Fifth Ed., California Polytechnic State University, Addison-Wesley Publishing Company, New York, 1998.

37. Shapiro, A.R., R.F. Lutomirski, H. T. Yura, "Induced Fields and Heating Within a Cranial Structure Irradiated by an Eiectromagnetic Plane Wave," *IEEE Transactions on Microwave Theory and Techniques*, Vol. MTT-19, no. 2, pp. 187-196, February 1971.

38. Weil, C.M., "Absorption Characteristics of Multilayered Sphere Models Exposed to UHF/Microwave Radiation," *IEEE Transactions on Biomedical Engineering*, Vol.BME22, no. 6, pp. 468-476, November 1975.

39. Balanis, C.A., *Antenna Theory, Analysis and Design,* John Wiley & Sons, New York, 1982.

40. Burkhardt, M., Y. Spinelli, N. Kuster, "Exposure Setup to Test Effects of Wireless Communication Systems on the CNS," *Health Physics*, Vol. 73, no. 5,pp. 770-778, November 1997.

41. Çelik, C.G., "EM Effects of Mobile Phone on Humanbeing," MS. Thesis, Boğaziçi University, 2001.

REFERENCES NOT CITED

1. Lin, J.C., "Research on Health from Cell Phone Radiation, Telecommunications Health & Safety," *IEEE Antennas and Propagation Magazine*, Vol. 42, no.4, August 2000.

2. Fabiano, B., C. Marco, D.Daniele, G.Domenico, G.Paolo, "Electromagnetic Fields in Proximity of GSM Base Stations," *Proceedings of the International Wroclaw Symposium on Electromagnetic Compatibility*, June 23-25, 2000, pp. 250-254, Wraclow, Poland, 2000.

3. Taurisano, M.D., A.V. Vorst, "Experimental Thermographic Analysis of Thermal Effects Induced on a Human Head Exposed to 900 MHz Fields of Mobile Phones," *IEEE Transactions on Microwave Theory and Techniques*, Vol. 48, no.11, pp. 2022-2032, November 2000.

4. Nelson D.A., M.T. Nelson, T.J. Walters, P.A. Mason, "Skin Heating Effects of Millimeter-Wave Irradiation-Thermal Modeling Results," *IEEE Transactions on Microwave Theory and Techniques*, Vol. 48, no. 11, pp. 2111-2120, November 2000.

5. Caputa, K., M.A. Stuchly, "Evaluation of Electromagnetic Interference from a Cellular Telephone with a Hearing Aid," *IEEE Transactions on Microwave Theory and Techniques*, Vol. 48, no. 11, pp. 2148-2154, November 2000.

6. Apollonio, F., M. Liberti, G. d'Inzeo, L. Tarricone, "Integrated Models for the Analysis of Biological Effects of EM Fields Used for Mobile Communications," *IEEE Transactions on Microwave Theory and Techniques*, Vol. 48, no. 11, pp. 2082-2092, November 2000.

7. Moulder, J.E., "Cellular Phone Antennas and Human Health, Electromagnetic Fields and Human Health," *http://www.mcw.edu/gcrc/cop/cell-phone-health-Faq/toc*.

8. Iqbal, O., "Warning: Cellular Communication May Damage Your Health," *http://www-dse.doc.ic.ac.uk*.